UNIVERSITY OF BASEL

Department of Chemistry Prof. Dr. John P. Maier, FRS Klingelbergstrasse 80 Tel. +41 61 267 38 26 (or 00)
CH-4056 Basel Fax +41 61 267 38 55
Switzerland E-Mail J.P.Maier@unibas.ch

http://www.chemie.unibas.ch/~maier

Final report: IRI Project: contract no. F61775-02-C4029, June 2002-May 2005

The broad objectives of this IRI project which ran during three years, June 2002- May 2005, were the investigations of the spectroscopic properties of boron species, their aggregation and reactions in matrices ranging from neon to those doped with hydrogen. The studies of the aggregation properties were hampered by the lack of spectroscopic knowledge on the electronic transitions of the polyatomic boron molecules and their ions. Thus it was clear that their identification at first had to be undertaken in order to proceed on this. The same applies to reactions in hydrogen dopped matrices. This was accomplished for B_3 and B_3^-. In addition theoretical predictions for the future studies of the B_4 species and its positive and negative ions were completed. The project was initially instigated on the advice and recommendation of Dr.C.W.Larson, AFRL, Edwards Air Force Base, California, whose continual guidance, suggestions and enthusiasm throughout the project were much appreciated.

For the purpose of the spectral identification and characterisation of polyatomic boron molecules, a world-wide unique apparatus, combining mass-selection (using a cesium sputter source) with a matrix isolation technique was initially used, backed up by theoretical calculations. The six, 6-month interim reports summarized the experiments undertaken, including the unsuccessful ones. Because the electronic spectra of the triatomic boron species were identified in 5 K neon matrices, an ambitious project to observe the gas phase spectrum of B_3 could also be realized.

The project as a whole proved rather successful and productive as evidenced by 5 publications during this three year period in leading journals of chemical physics:

“Electronic absorption spectra of B_3 and B_3^- in neon matrices and ab initio analysis of the vibronic structure”
M.Wyss, E.Riaplov, A.Batalov, J.P.Maier, T.Weber, W.Meyer and P.Rosmus
Journal of Chemical Physics, **119**, 9703, 2003.

“Gas phase detection of cyclic B_3: $^2E' - X\,^2A_1'$ electronic origin band“
P.Cias, M.Araki, A.Denisov and J.P.Maier
Journal of Chemical Physics, **121**, 6776, 2004.

Report Documentation Page

Form Approved
OMB No. 0704-0188

1. REPORT DATE	2. REPORT TYPE	3. DATES COVERED
28 JUN 2005	**N/A**	**-**

4. TITLE AND SUBTITLE	5a. CONTRACT NUMBER
Characterization of Boron Atom Aggregation	5b. GRANT NUMBER
	5c. PROGRAM ELEMENT NUMBER
6. AUTHOR(S)	5d. PROJECT NUMBER
	5e. TASK NUMBER
	5f. WORK UNIT NUMBER
7. PERFORMING ORGANIZATION NAME(S) AND ADDRESS(ES) **University of Basel Klingelbergstrasse 80 Basel CH-4056 Switzerland**	8. PERFORMING ORGANIZATION REPORT NUMBER
9. SPONSORING/MONITORING AGENCY NAME(S) AND ADDRESS(ES)	10. SPONSOR/MONITOR'S ACRONYM(S)
	11. SPONSOR/MONITOR'S REPORT NUMBER(S)

12. DISTRIBUTION/AVAILABILITY STATEMENT
Approved for public release, distribution unlimited

13. SUPPLEMENTARY NOTES
The original document contains color images.

14. ABSTRACT

15. SUBJECT TERMS

16. SECURITY CLASSIFICATION OF:			17. LIMITATION OF ABSTRACT	18. NUMBER OF PAGES	19a. NAME OF RESPONSIBLE PERSON
a. REPORT	b. ABSTRACT	c. THIS PAGE			
unclassified	**unclassified**	**unclassified**	**UU**	**37**	

Standard Form 298 (Rev. 8-98)
Prescribed by ANSI Std Z39-18

"The near infrared $1^2A_2'' - X\ ^2A_1'$ electronic transition of B_3 in a neon matrix"
A.Batalov, J.Fulara, I.Shnitko and J.P.Maier
Chemical Physics Letters, **404**, 315, 2005.

"Vibrations in the B_4 rhombic structure"
R. Linguerri, I.Navizet, P.Rosmus, S.Carter and J.P.Maier
Journal of Chemical Physics, **122**, 34301, 2005.

"Theoretical study of the electronic excited states of B_4, B_4^+ and B_4^- "
C.Gillery, R.Linguerri, P.Rosmus and J.P.Maier
Z. Phys.Chem., **219**, 467, 2005.

These five publications summarize the results and success of this IRI project and are included with this report.

The project involved experimental studies using our special matrix apparatus in Basel with which a number of PhD students worked during this period, starting with M.Wyss, E.Riaplov (both PhD now) and continued by A.Batalov, I.Shnitko. They were assisted in the experiments by the annual visits of Dr.J.Fulara, a long standing collaborator from the Polish Academy of Sciences, Warsaw, and succeeded in the measurement of the electronic spectra of B_3 and B_3^- in neon matrices. As a follow up to this the gas phase spectrum of B_3 was obtained by the students P.Cias (now PhD), A.Denisov, working under the guidance of Dr.M.Araki.

The interpretation of the vibronic structure and symmetry of the electronic transitions of B_3 and B_3^- proved possible as result of extensive collaborations with two theoretical groups: that of Prof.P.Rosmus, University of Marne la Vallee, France and Prof.W.Meyer, University of Kaiserslautern, Germany. P.Rosmus spent 1-2 month periods in each of the three years of this IRI project as a guest Professor here working on the structure and spectroscopy of boron species, predicting their geometric, electronic and vibrational patterns. Two of his PhD students (C.Gillary, R.Linguerri) also had sojourns in Basel and these theoretical studies are a major part of their theses.

Though the IRI project has come to an end, we plan to continue our spectroscopic studies of the boron clusters. Specifically the tetraatomic and larger boron molecules could be studied in the gas phase by multiphoton ionisation and laser induced fluorescence methods- the instrumentation for which is available in our laboratory in Basel- combined with a laser ablation source. For the neon matrix experiments a new ion source, incorporating a high repetition laser vaporization design, for the deposition of the larger boron ions is in construction.

EOARD is thanked gratefully for providing this three year contract which has enabled us to open up a new area of research for boron clusters, led to multi-national collaborations and resulted in interactions and possible projects for the future with several groups in the U.S.A. on such and related research.

“The Contractor, Professor John P.MAIER, hereby declares that, to the best of his knowledge and belief, the technical data delivered herewith under contract No. F61775-02-C42029 is complete, accurate and complies with all the requirements of the contract”

Date: Basel 26. June 2005

Name and Title of Authorized Official: Professor John P.Maier

“I certify that there were no subject inventions to declare as defined in FAR 52.227-13, during the performance of this contract”

Date: Basel 26. June 2005

Name and Title of Authorized Official: Professor John P.Maier

Electronic absorption spectra of B_3 and B_3^- in neon matrices and *ab initio* analysis of the vibronic structure

Muriel Wyss, Evgueni Riaplov, Anton Batalov, and John P. Maier[a)]
Department of Chemistry, University of Basel, Klingelbergstrasse 80, CH-4056 Basel, Switzerland

Thomas Weber and Wilfried Meyer
Department of Chemistry, University of Kaiserslautern, Erwin-Schroedinger-Strasse 52/527, D-67663 Kaiserslautern, Germany

Pavel Rosmus
Laboratoire de Chimie Théorique, Université de Marne la Vallée, F-77454 Champs sur Marne, France

(Received 17 July 2003; accepted 4 August 2003)

Mass selected B_3^- ions have been isolated in 6 K neon matrices and their absorption spectra measured. A band system with origin at 467 nm is assigned as the $^1E' \leftarrow X\,^1A_1'$ electronic transition of the cyclic anion. After photobleaching, the $1\,^2E' \leftarrow X\,^2A_1'$ and $2\,^2E' \leftarrow X\,^2A_1'$ band systems of neutral cyclic B_3 are observed which start around 736 and 458 nm, respectively. Large scale *ab initio* calculations have provided potential energy surfaces for a variational treatment of the vibrational motion. Calculated band origins leave no doubt about the electronic symmetry assignments. The complex vibrational structure in the $1\,^2E'$ state, which is due to relatively strong Jahn–Teller distortions, appears to be closely reproduced by the calculated vibrational energies and intensities, if the first observed stronger line is identified with the first vibrationally excited state, placing the ''true'' band origin of the $1\,^2E'$ state at 775 nm where no signal with significant strength is apparent. The $2\,^2E'$ state undergoes only a relatively weak Jahn–Teller distortion and shows a short progression with an observed frequency of 981(10) cm^{-1} that compares favorably with the theoretical frequency of 973 cm^{-1}. The $^1E'$ system of B_3^- shows a Jahn–Teller activity comparable to that of the $1\,^2E'$ state of B_3. © *2003 American Institute of Physics.* [DOI: 10.1063/1.1613251]

I. INTRODUCTION

There has been a growing interest in the structure and energetics of small boron and boron containing molecules because they have a variety of applications such as for the construction of high temperature semiconductor devices, as chemical insulators, and in the production of refractory materials and explosives.[1] However, there is little information on the spectroscopy of pure boron species in the literature. Only the boron dimer[2] and its anion[3] appear to be well characterized experimentally and theoretically.

Two experimental studies have been carried out for B_3, both in rare-gas matrices. One of these is an electron spin resonance (ESR) investigation that has confirmed the presence of three equivalent nuclei in the $^2A_1'$ ground state[4] and the other is an infrared spectroscopic study in which the degenerate mode (e') has been observed for both $^{11}B_3$ and $^{10}B_3$ isotopomers (886 and 928 cm^{-1}, respectively).[5] Several theoretical investigations on the B_3 molecule have predicted an equilateral cyclic structure (D_{3h}) with a $^2A_1'$ electronic symmetry,[6–9] and the vibrational frequencies in the electronic ground state. Of the low-lying excited electronic states, only the states of $^2A_2''$ and $^2E'$ symmetry are accessible from the $^2A_1'$ ground state by dipole allowed excitation. Several transition bands are expected in the near infrared and visible regions.[7,8] Because the Jahn–Teller distortion in the E states implies stretching of a strong bond, the B_3 molecule should provide a very interesting example for vibrational motion that proceeds on two coupled surfaces even for the lowest vibrational quanta.

Data on the B_3^- anion are even more scarce. There is only a theoretical study predicting a linear $^1\Sigma_g^+$ electronic ground state for this species from MP4 calculations.[9] However, MR-CI calculations carried out as part of this work show clearly that the lowest energy isomer possesses a cyclic D_{3h} structure with a $^1A_1'$ electronic ground state. As far as larger negatively charged boron molecules are concerned, only the gas phase photoelectron spectrum of B_5^- has been reported.[10]

In the present work the electronic absorption spectra of B_3^- and B_3 have been measured in neon matrices at 6 K following mass-selection. In order to provide symmetry assignments and an interpretation of the complex vibronic structure observed in the excited electronic state $1\,^2E'$ of B_3 as result of the Jahn–Teller effect, multireference configuration interaction (MR-CI) *ab initio* electronic structure calculations have been undertaken. Based on diabatic potential energy surfaces in analytical form, the vibrational motion has been analyzed in variational calculations using hyperspherical coordinates. For the lower transition of B_3, line intensities and a tentative vibronic assignment are presented.

II. EXPERIMENT

The apparatus employed has been described previously.[11] The B_3^- anions were produced in a cesium sput-

a)Author to whom correspondence should be addressed. Fax: +41-61-267-38-55. Electronic mail: j.p.maier@unibas.ch

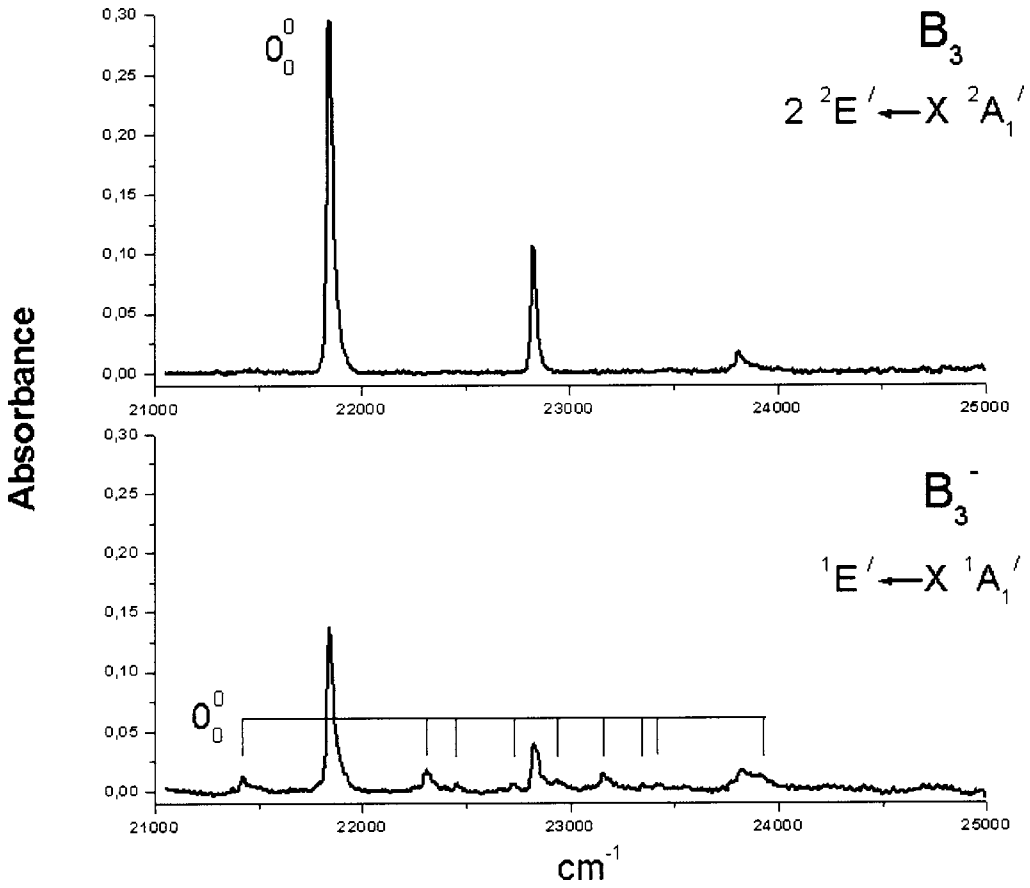

FIG. 1. Electronic absorption spectra recorded in a 6 K matrix after 4 hours of mass-selected codeposition of B_3^- with neon. The bottom trace shows the $^1E'-X\ ^1A_1'$ electronic transition of B_3^- overlapped by the $2\ ^2E'-X\ ^2A_1'$ system of B_3, produced from partial neutralization of the anions impinging on the matrix during deposition. The top trace reveals the $2\ ^2E'-X\ ^2A_1'$ electronic transition of B_3 measured after exposure to UV radiation. Absorption belonging to the anion disappears.

ter ion source that had been built originally for the production of carbon anions.[12] A boron-carbide (B_4C) rod or pressed pure boron powder were used as sputter targets. The ions produced in the source were guided by an electrostatic lens system into a quadrupole mass analyzer, where the B_3^- anions were selected and then codeposited with excess of neon onto a rhodium coated sapphire plate at a temperature of 6 K. Ion currents of 25 nA using the boron sputter target and 10 nA from B_4C could be obtained for the mass selected $^{11}B_3^-$ anions with unity mass resolution. All the experiments but one were performed with the B_4C precursor because the available pure boron sample was brittle.

Matrices of about 150 μm thickness were grown during 4 hours. Absorption measurements in the 220–1100 nm range were carried out by passing monochromatic light from a halogen or xenon arc lamp through the matrix employing a waveguide-like technique and achieving a path length of about 2 cm. A medium pressure mercury lamp ($E \leqslant 5.4$ eV) was used to neutralize the trapped ions. After exposure to the UV radiation the spectra were recorded again.

III. OBSERVATIONS

A. Absorption system

Three unknown systems built upon the apparent band origins at 458, 467, and 736 nm were observed after mass selected (33 u) codeposition of B_3^- ions with neon. As is illustrated by Fig. 1, exposure of the matrix to 5.4 eV radiation resulted in the complete disappearance of the 467 nm system and the growth of the 458 nm one. In addition, a new system starting at 736 nm evolved (Fig. 2), exhibiting a rich vibrational structure and correlating in intensity with the 458 nm one. Thus one concludes that the carrier of the 467 nm system is the B_3^- anion, whereas the 458 and 736 nm band groups are due to the neutral B_3 species. Because natural boron contains about 20 percent as its ^{10}B isotope, it was reasonable to check whether or not some of these newly observed absorptions belong to the B_2C molecule or its ion. This molecule is also produced in the cesium sputter source from a B_4C rod and its $^{10}B^{11}BC$ isotopomer has the same mass as B_3 and is, therefore, deposited as well. Nevertheless, even after deposition of $^{11}B_2C^-$ (34 u), the production of which is much higher than that of $^{10}B^{11}BC^-$, neither of the above described systems were seen while usage of a pure boron rod in the source led again to the detection of the three band systems of Figs. 1 and 2 with the same intensity ratios. This supports the assignment of the absorptions observed to the B_3 molecule and its anion.

The equilateral triangle structure of the neutral molecule B_3 in the ground electronic state of $^2A_1'$ symmetry is well established.[9] Dipole transition moments of symmetry A_2''

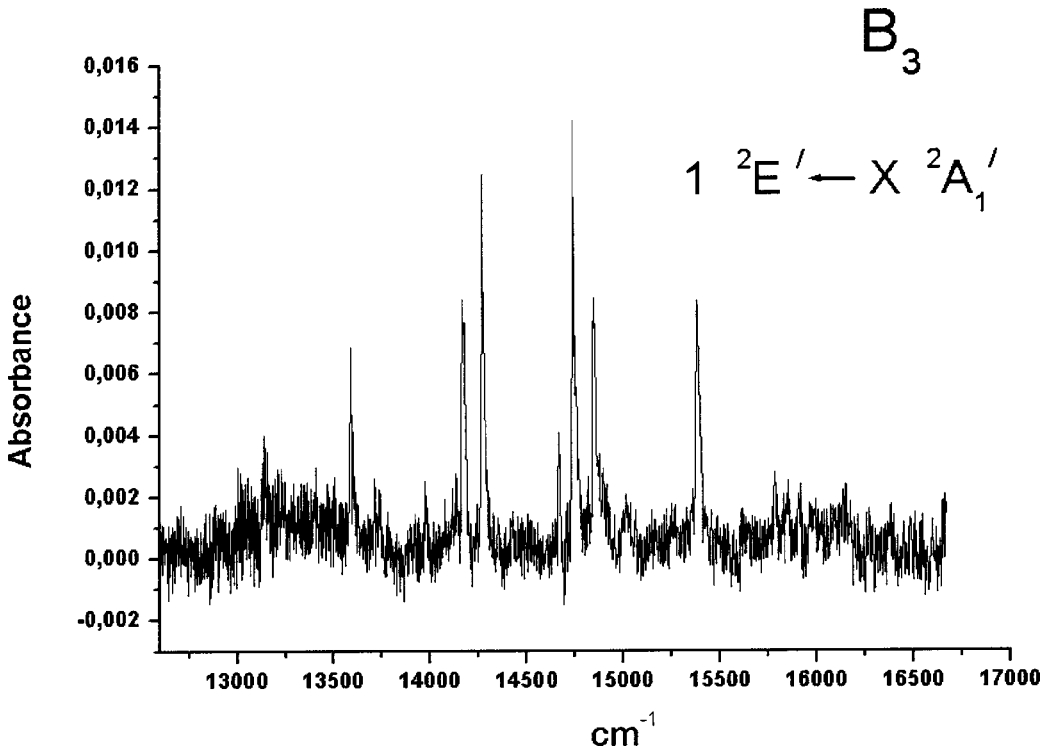

FIG. 2. Electronic absorption spectrum of the $1\,^2E'-X\,^2A_1'$ electronic transition of B_3 recorded after 4 hours of mass-selected codeposition with neon followed by UV irradiation of the 6 K matrix.

$+E'$ connect this state only with states of symmetry $^2A_2''$ and $^2E'$, respectively. As argued in detail later on, only $^2E'$ states are available in the range of excitation energies investigated here.

Because the cyclic B_3 neutrals are produced by photodetachment of the electron from the mass-selected B_3^- and isomerization of a linear to cyclic form of species held relatively rigidly in a 6 K neon lattice on irradiation with 3–5 eV photons is unlikely, the measured electronic spectrum of B_3^- is also ascribed to a cyclic isomer with ground state of $^1A_1$ symmetry. This is in line with the observation that the excitation energy is close to the corresponding transition in neutral B_3, as to be expected from simple molecular orbital (MO) considerations since the same MOs are involved and the theoretical prediction for the transition (see Sec. IV). Therefore, the upper state of the band system observed is assigned to the $^1E'$ electronic symmetry.

B. Vibrational structure

The vibrational structure apparent in the observed electronic spectra (Figs. 1 and 2 and Tables I–III) is associated with excitation of the two normal modes, $\nu_1(a_1')$, $\nu_2(e')$, in the upper electronic states because at 6 K the population is essentially all in the vibrationless level of the ground state. Because the upper electronic states of B_3 and B_3^- have E' symmetry they are subject to Jahn–Teller distortions which may cause complex vibrational pattern.

The second system of B_3, assigned to the $2\,^2E'\leftarrow X\,^2A_1'$ transition, has the simplest pattern: Starting with the origin band at 458 nm a seemingly regular progression mode is discernible (Fig. 1) with two spacings that are the same within the error limit (Table III). As the origin band is dominant, no large geometry change is expected on passing from the ground to the excited electronic state.

In contrast, the vibronic structure of the first system of B_3 (Fig. 1, top trace, Table II), assigned to the $1\,^2E'\leftarrow X\,^2A_1'$ transition, indicates a strong Jahn–Teller distortion: The excitation of the degenerate $\nu_2(e')$ Jahn–Teller active mode is evident. The two transition systems are not only very different in complexity, they also show quite different intensities: The spectra indicate an absorbance ratio of one order of magnitude in favor of the second band.

The absorption spectrum of B_3^- (Fig. 2, bottom trace, Table I), assigned to the $1\,^1E'\leftarrow X\,^1A_1'$ transition, shows a complexity similar to the lower transition of B_3. The patterns of these two systems are really not simple and a sensible assignment can only be made by means of a theoretical treatment as attempted in Sec. V.

TABLE I. Positions of band maxima ($\lambda \pm 0.2$ nm) observed in the $1\,^1E'-X\,^1A_1'$ absorption spectrum of B_3^- in a 6 K neon matrix

λ (nm)	ν (cm^{-1})	$\Delta\nu$ (cm^{-1})
466.9	21 412	0
448.4	22 295	883
445.5	22 440	1028
440.2	22 711	1299
436.2	22 919	1507
431.9	23 147	1735
428.4	23 336	1924
427.1	23 407	1995
418.4	23 894	2482

TABLE II. Positions of band maxima ($\lambda \pm 0.2$ nm) in the $1\,^2E'-X\,^2A_1'$ absorption spectrum of B_3, vibronic symmetry Γ and calculated intensities.

		$\Delta\nu(\mathrm{cm}^{-1})$				
λ(nm)	$\nu\,(\mathrm{cm}^{-1})$	Experiment[a]		Theory	Γ	Intensity
				0	E'	1.00
				230	A_1'	
735.8	13 587	0	685	685	E'	1.45
				733	A_2'	
715.5	13 972	385	1070	1074	E'	0.74
				1073	A_1'	
705.6	14 168	581	1266	1269	E'	0.59
700.7	14 268	681	1366	1337	E'	1.80
				1425	A_1'	
				1660	A_2'	
681.6	14 667	1080	1765	1732	E'	0.25
678.3	14 739	1152	1837	1818	E'	1.70
				1801	A_1'	
				1910	A_2'	
673.4	14 846	1259	1944	1933	E'	0.60
				2123	E'	0.20
				2195	A_1'	
				2202	E'	0.01
				2310	E'	0.00
				2340	A_2'	
				2384	A_1'	
650.0	15 380	1793	2478	2444	E'	0.98
				2481	E'	0.01
				2537	A_1'	
				2564	A_1'	
				2648	A_2'	
				2714	A_2'	
				2728	E'	0.03
				2762	A_1'	
				2834	E'	0.11
				2848	E'	0.04
				2868	A_2'	
				2915	A_1'	
				2920	E'	0.45
				3057	E'	0.02

[a]For two different band origins, see text.

TABLE III. Positions of band maxima ($\lambda \pm 0.2$ nm) observed in the $2\,^2E'-X\,^2A_1'$ absorption spectrum of B_3, calculated vibrational energies and vibronic symmetry Γ.

		$\Delta\nu(\mathrm{cm}^{-1})$		
λ(nm)	$\nu\,(\mathrm{cm}^{-1})$	Expt.	Theory	Γ
458.0	21828	0	0	E'
			848	A_2'
438.3	22809	981	973	E'
			974	A_1'
			1258	E'
			1746	E'
			1815	A_2'
420.1	23797	1969	1951	E'
			2018	A_1'
			2144	E'

IV. THEORY

Symmetry assignments and analysis of complex vibrational structures as observed for B_3 require the knowledge of sufficiently accurate and extended potential energy surfaces (PES) for low-lying electronic states. Because previous theoretical efforts have been limited to a few cuts through selected PESs,[7] we have performed large-scale *ab initio* calculations for the states relevant to the absorption spectra presented here.[13]

The orbital ordering for B_3 in D_{3h} symmetry is $1a_1'$, $1e'$, $2a_1'$, $2e'$, $1a_2''$, $3a_1'$ for the orbitals occupied in the ground state, and $3e'$, $1e''$, $4e'$, $1a_2'$,... for the lower virtual orbitals. Clearly, the ground state is of $^2A_1'$ symmetry and excited states accessible by dipole selection rules have $^2A_2''$ and $^2E'$ symmetries. While the $1\,^2A_2''$ state is dominated by the single configuration resulting from the $3a_1'\leftarrow 1a_2''$ excitation, two low-lying $^2E'$ states should result from substantial mixing of the configurations corresponding to the excitations $3e'\leftarrow 3a_1'$ and $3a_1'\leftarrow 2e'$, respectively. The ground state configuration of B_3^- is that of B_3 but with an extra electron in the highest occupied orbital $3a_1$. The lowest dipole allowed excitation is here dominated by the $3e'\leftarrow 3a_1'$ promotion.

A configuration mixing as indicated above, on top of the interaction between the two components of the $^2E'$ states for distorted C_s geometries where both have $^2A'$ local symmetry, restricts our choice of method effectively to the variational multireference configuration interaction (MR-CI) procedure. For efficiency we use a complete active space (CASSCF) for the reference wave functions and the internally contracted singles and doubles CI, as implemented in the MOLPRO[14] program package. The whole set of geometries is treated with an active space spanned by the orbital set from $2a_1'$ to $1e''$; extended calculations for a subset of C_{2v} geometries use an active space that includes the $4e'$ and $1a_2'$ orbitals as well. The basis set is constructed from the augmented correlation-consistent valence triple zeta (aug-cc-pVTZ) set for the B atom,[15] further augmented by two *s* functions (exponents 0.7 and 0.23) and one *p* set (exponent 0.35) at the bond centers. Comparison between experiment and theory for B_2 suggests that this computational procedure supports an accuracy of about 0.02 bohr in bond lengths and about 20 cm^{-1} in vibrational frequencies. These calculations have been performed for a grid of geometries which was defined by bond length variations in steps of 0.05 bohr, starting from the reference bond length of $r=3.00$ bohr and extending to all geometries for which one of the relevant electronic energies was less than 3000 cm^{-1} above the corresponding reference energy.

The adiabatic PES's have been cast in analytical form by least-squares fits to polynomials in the symmetric stretch and radial deformation coordinates and harmonic functions of the azimuthal deformation coordinate, as described in previous work on alkali trimers.[16,17] In contrast to the alkali trimers, Jahn–Teller distortion in the lower E' states of B_3 and B_3^- is weak as compared to vibrational excitation, so that both sheets of the PES for degenerate *E* states are substantially populated even for low vibrational energies. In order to avoid the notorious complications caused by the geometric phase in an adiabatic treatment, we use a diabatic framework for the vibrational motion, i.e., diabatic surfaces are constructed from the adiabatic ones by means of 2×2 rotations with

angles $\phi/2$, where ϕ is the pseudo-rotational coordinate. Hyperspherical coordinates are still the proper choice for a cyclic trimer but the computational procedures used previously[18] had to be extended to account for pairs of coupled diabatic surfaces. Both, the analytical fits and the vibrational calculations introduce numerical errors in the order of only 1 cm^{-1} for the first transition in B_3, i.e., considerably smaller errors than those from the electronic structure calculations. For the other upper states our fits with standard errors of about 10 cm^{-1} are only preliminary because of complications from additional conical intersections and/or notorious intruder state problems which cause unphysical humps in the upper state surfaces in particular for B_3^-.

Vibrational line intensities are calculated from transition dipole moment surfaces which are again expanded in polynomials as outlined above for the PES. Because the observed bands stem from in-plane transition moments (parallel bands), vibronic selection rules leave only $^2E'$ vibronic states accessible in the case of free B_3. The degree of violation of this selection rule due to matrix effects is difficult to assess.

A sensible assignment of vibronic states by some kind of vibrational quantum numbers is difficult in cases of strong vibronic coupling, i.e., if linear and quadratic Jahn–Teller (JT) terms are of comparable size. Reference can be made to two simple limiting cases: (i) Strong quadratic terms produce three equivalent minima on the lower (adiabatic) surface which are separated by a relatively high barrier. The vibrational wave functions for the lower sheet can then be considered a linear combination of three equivalent local vibrators with C_{2v} symmetry placed at the respective minima and can be labeled by C_{2v} quantum numbers v_1, v_2, and v_3 for symmetric stretch, symmetric bend and asymmetric stretch, respectively. (ii) Weak quadratic JT terms produce only negligible localizing barriers for the pseudorotational motion. Then the quantum numbers for a free internal rotation are adequate, i.e., v_1, v_2 for symmetric stretch and deformation and l_2 for the pseudorotation angular momentum. In an adiabatic frame, v_2 and l_2 are half integer numbers due to the geometric phase in electronic and vibrational factors of the vibronic wave function. The finger print for case (i) is a near degeneracy of *E-A* pairs, that for case (ii) is a near degeneracy of A_1-A_2 pairs. The actual assignment of model quantum numbers is made by inspection of plots of the vibrational wave functions. The model following case (i) has been successfully used for rovibronic analysis of alkali trimer $E''\leftarrow E'$ transition bands;[16–18] a thorough discussion of this model has been given there. Further details of our computational procedures may be found elsewhere.[13]

V. ASSIGNMENT AND DISCUSSION

Our CAS-SCF calculations of vertical electronic transition energies at the D_{3h} reference geometry (bond length 3.00 bohr) reproduce the ordering of states as previously obtained, also from CAS-SCF:[9] $X\,^2A_1'$, $1\,^2A_2''$, $1\,^2E'$, $1\,^4E''$, $1\,^4E'$, $1\,^2E''$, $2\,^2E'$, $1\,^4A_1'$, $1\,^4A_2'\ldots$. Pertinent data of the PESs, as obtained in the MR-CI calculations for the states relevant here, are collected in Table IV. Figure 3 shows cuts of these potentials for the bending deformation mode, which illustrate in particular the Jahn–Teller distortions in the E' states. The JT stabilization in the $1\,^2E'$ state of 475 cm^{-1} is on the order of stabilizations observed for alkali trimer $^2E''$ states, but it amounts to little more than 1/3 of the zero point energy and only about 2/3 of the deformation mode energy quantum. The pseudorotational barrier between the three equivalent minima is only 187 cm^{-1} but it is sufficiently broad to effectively lift the A_1/A_2 degeneracy, indicating a case (i) description of the vibronic states. In contrast, for the $2\,^2E'$ state with stabilization and localization energies of only 39 and 9 cm^{-1}, respectively, B_3 can be considered as

TABLE IV. Transition energies, Jahn–Teller distortion energies and equilibrium geometries for selected states of B_3 from MR-CI with the large active space (energies in cm^{-1}, distances in bohr and angles in degree).

State:	$1\,^2A_1'$	$1\,^2E'$	$2\,^2E'$
T_v		13 781	22 291
T_e		13 057	22 202
T_{00}		12 829	22 272
ZPE	1457	1207	1522
E_{stab}		475	39
E_{loc}		187	9
r_{min}	2.968	2.982	3.015
θ_{min}	60.0	65.3	61.9
r_{sadd}		3.093	2.982
θ_{sadd}		57.2	60.9

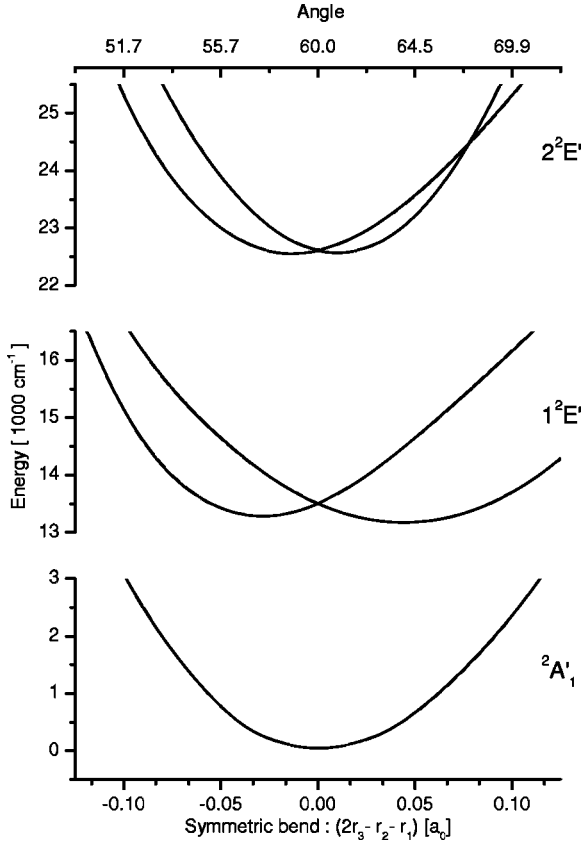

FIG. 3. One-dimensional cuts of the PESs along the bend coordinate for C_{2v} geometries with $(r_1+r_2+r_3)/3=3.00$ bohr for the $X\,^2A_1'$ and the two $^2E'$ electronic states of B_3.

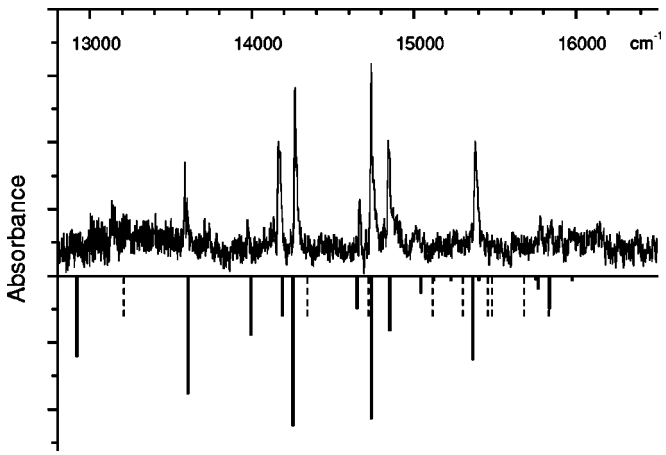

FIG. 4. Comparison of the calculated positions and intensities of the Jahn–Teller coupled vibronic levels for the $1\,^2E'$ state of B_3 with the matrix spectrum.

nearly freely pseudo-rotating, indicating a case (ii) description. This state has a second conical intersection of its two electronic components at C_{2v} geometries with apex angles around 68°. Such a feature causes severe complications for the fitting of a PES. Our present analytical potential is reliable only below that crossing and furnishes but a few low-lying vibrational levels. The shapes of these PES, and even more so the rather unexpected shapes of the transition moment surfaces, are consequences of the strong mixing of the two configurations that are formed by the $3e' \leftarrow 3a_1'$ and the $3a_1' \leftarrow 2e'$ excitations. Actually, at the D_{3h} reference geometry the mixing ratios are 62:58 and 61:59 for the $1\,^2E'$ and $2\,^2E'$ states, respectively. The corresponding dipole transition moments of 0.137 and 0.253 a.u., respectively, indicate a clear difference in the intensities of the two bands, as is indeed observed.

The calculated positions of the transition bands are crucial for the assignment of electronic symmetries. We find the $1\,^2E'$ band origin, T_{00}, at 12 829 cm^{-1} from the MR-CI with extended reference space. The corresponding results from the smaller MR-CI and from a Davidson correction are 12 988 and 12 728 cm^{-1}, respectively, indicating an uncertainty in T_{00} of about 250 cm^{-1}. However, the observed spectrum starts with a line at 13 587 cm^{-1}, which is 752 cm^{-1} higher than calculated. This difference is too large to be attributed to matrix effects. It is not only larger than the estimated uncertainty, but its sign is unlikely since in variational calculations excited-state energies are usually less well accounted for than ground-state energies. This suggests that the first observed line is not the band origin but corresponds to the first excited vibrational level. This is indeed supported by the positions and intensities calculated for the higher vibrational states, as obvious from Fig. 4, where the observed spectrum is compared with the theoretical one, the latter shifted only by 30 cm^{-1}. Agreement appears to be rather satisfactory considering the well-known fact that matrix effects may affect the band positions and in particular their intensities. The triplet feature seen in the center of the spectrum belongs to vibrational states that are heavily mixed, so that the calculated intensities may well need some redistribution, since the composition of the vibronic wave functions is computationally more sensitive to the accurate description of the coupling than the vibronic energies. However, this assignment of the vibrational structure is in conflict with the fact that the observed spectrum does not show a line with significant strength at the predicted position of the band origin. On the other hand, if the band origin is identified with the first strong observed line, we can not explain that two strong observed lines do not have theoretical counterparts and that a line with a strong calculated intensity is missing. It is difficult to see how matrix effects could be held responsible for this mismatch. A gas spectrum is necessary.

Table II lists observed and calculated vibrational energies and the calculated relative intensities, making also use of the theoretical first excitation energy to define the ''true'' band origin, which becomes 12 902 cm^{-1}. Figure 5 displays vibrational levels ordered according to vibronic symmetry and assigned with vibrational quantum numbers of a C_{2v} vibrator as outlined above. This assignment is reasonable for the lower levels but loses meaning for higher ones, in particular if levels are close and undergo substantial mixing. This is regularly the case for neighboring levels of polyads formed by replacing two quanta of symmetric bend by one quantum of asymmetric stretch. Note that only the levels of vibronic E character are accessible.

The calculated band origin for the $2\,^2E'$ state of 22 272 cm^{-1} agrees fairly well with the observed position of the main line, 21 828 cm^{-1}. There is no other candidate close by. Vibrational energy levels, which are only preliminary in this case due to problems with the fit of the PES, are included in Table III. The observed line positions may be nicely lined up with calculated values but this is not really definitive as long as theoretical intensities are lacking for this state. While the ground vibrational state is 93% a_1', the first upper state is 60% e_1' and 30% a_1', i.e., the progression observed involves mainly the deformation mode with only zero-point pseudorotation. The proper assignment according to case (ii) is (0 1/2 1/2), (0 3/2 1/2), and (0 5/2 1/2) for the three levels involved.

For the $1\,^2A_2'$ state we calculate a vertical excitation energy T_v of 6300 cm^{-1}. This region was inaccessible in the experiments carried out hitherto. As a general comment on the transition energies, we note that dynamical electron correlation, accounted for only by the singles–doubles CI build on top of the CAS-SCF, causes changes of up to 2000 cm^{-1}. Comparison to previously published theoretical excitation energies, which are limited to CAS-SCF, shows indeed differences of this order.[8]

In the case of the B_3^- anion the calculated adiabatic excitation energy T_e of 23 089 cm^{-1} differs from the observed band origin at 21 413 cm^{-1} by 1676 cm^{-1}. Less than 300 cm^{-1} may be attributed to the change in the zero point energy (ZPE), leaving a defect of around 1400 cm^{-1}. Extension of our basis set by diffuse functions, which might be important for an excited state of an anion, reduces this defect by only about 100 cm^{-1} but the Davidson correction yields a surprisingly large further reduction of about 800 cm^{-1} in this case. The assignment to the $1\,^1E' \leftarrow X\,^1A_1'$ electronic transition of cyclic B_3^- is not questioned since no other candidates are available. A vibrational analysis of this transition has to

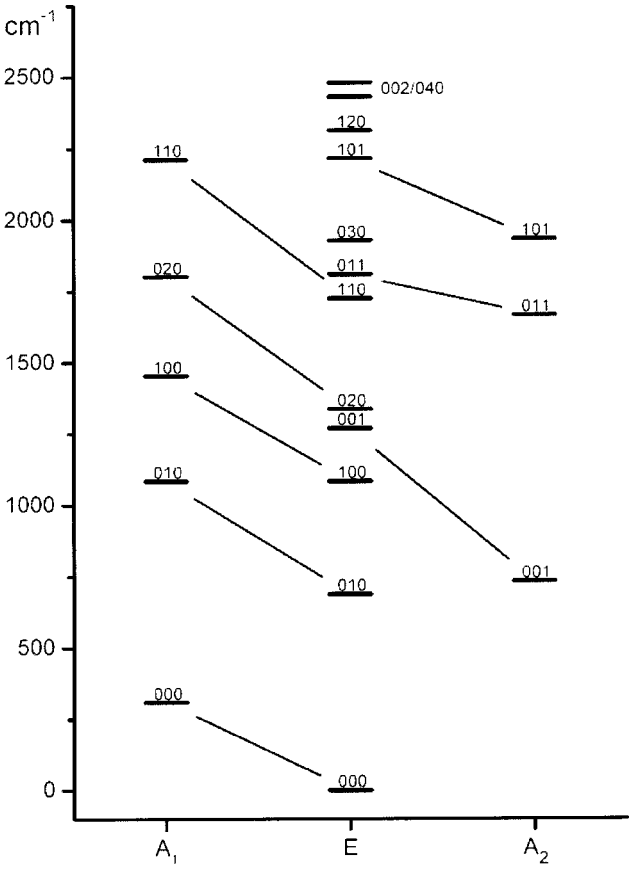

FIG. 5. Pattern of Jahn–Teller coupled vibronic levels of the $1\,^2E'$ state in B_3. For the definition of the modes see text.

be deferred until a better analytic representation of the upper state PES is available.

VI. CONCLUSION

The matrix isolation technique in combination with mass selection has been applied to observe for the first time the electronic spectra of the boron trimer and its anion. As a result, the $1\,^2E' \leftarrow X\,^2A_1'$ and the $2\,^2E' \leftarrow X\,^2A_1'$ electronic transitions for B_3 and $^1E' \leftarrow X\,^1A_1'$ for B_3^- have been identified. The vibronic structure of the $1\,^2E'$ electronic state of the neutral species and the $1\,^1E'$ state of the anion exhibit a strong influence of the Jahn–Teller effect. *Ab initio* calculations of potential energy surfaces for four electronic states of B_3 and two electronic states of B_3^- have validated the assignment of the observed bands and provided the basis for an analysis of the vibrational structure of the transition to the $1\,^2E'$ state of a free B_3. The observed pattern can be considered as well reproduced if the true origin of the transition is placed at about 12 900 cm^{-1} where no significant absorption line is seen. An in-depth analysis will require high resolution gas-phase measurements and theory developments. The present work provides the necessary basis for these to be undertaken.

ACKNOWLEDGMENTS

This study was financially supported by the Office of Aerospace Research and Development and the Swiss National Science Foundation (project 200020-100019). We thank Dr. C. W. Larson (U.S. Air Force Laboratory, Edwards Air Force Base, California) for all his help and suggestions with this project. We are indebted to Dr. S. Carter (Reading, UK) for making the program code for vibrational analysis capable to handle also a diabatic framework of electronic and vibrational motion.

[1] L. H. Hanley, J. L. Whitten, and S. L. Anderson, J. Am. Chem. Soc. **92**, 5803 (1988), and references therein.
[2] S. Tam, M. Macler, M. E. DeRose, and M. E. Fajardo, J. Chem. Phys. **113**, 9067 (2000), and references therein.
[3] K. P. Huber and G. Herzberg, *Constants of Diatomic Molecules* (Van Nostrand Reinhold, New York, 1979).
[4] Y. M. Hamrick, R. J. Van Zee, and W. J. Weltner, J. Chem. Phys. **96**, 1767 (1992).
[5] S. Li, R. J. VanZee, and W. J. Weltner, Chem. Phys. Lett. **262**, 298 (1996).
[6] J. M. L. Martin, J. P. Francois, and R. Gijbels, J. Chem. Phys. **90**, 6469 (1989).
[7] F. Marinelli and A. Pelegatti, Chem. Phys. Lett. **158**, 545 (1989).
[8] R. Hernandez and J. Simons, J. Chem. Phys. **94**, 2961 (1991).
[9] I. A. Howard and A. K. Ray, Z. Phys. D: At., Mol. Clusters **42**, 299 (1997).
[10] H.-J. Zhai, L.-S. Wang, A. N. Alexandrova, and A. I. Boldyrev, J. Chem. Phys. **117**, 7917 (2002).
[11] J. P. Maier, Chem. Soc. Rev. **26**, 21 (1997).
[12] D. Forney, J. Fulara, P. Freivogel, M. Jakobi, D. Lessen, and J. P. Maier, J. Chem. Phys. **103**, 48 (1995).
[13] T. Weber, Diploma, University of Kaiserslautern, 2001; T. Weber and W. Meyer (unpublished).
[14] MOLPRO is a package of *ab initio* programs written by H.-J. Werner and P. J. Knowles. Further information can be obtained from http://www.molpro.net.
[15] T. H. Dunning, J. Chem. Phys. **90**, 1007 (1989).
[16] H.-G. Krämer, M. Keil, C. B. Suarez, W. Demtröder, and W. Meyer, Chem. Phys. Lett. **299**, 212 (1999).
[17] M. Keil, H.-G. Krämer, A. Kudell, M. A. Baig, J. Zhu, W. Demtröder, and W. Meyer, J. Chem. Phys. **113**, 7414 (2000).
[18] S. Carter and W. Meyer, J. Chem. Phys. **93**, 8902 (1990); **100**, 2104 (1994).

Gas phase detection of cyclic B_3: $2\,^2E' \leftarrow X\,^2A_1'$ electronic origin band

P. Cias, M. Araki, A. Denisov, and J. P. Maier[a)]
Department of Chemistry, University of Basel, Klingelbergstrasse 80, CH-4056 Basel, Switzerland

(Received 29 January 2004; accepted 19 July 2004)

The rotationally resolved origin band in the $2\,^2E' \leftarrow X\,^2A_1'$ electronic spectrum of cyclic B_3 has been observed by cavity ring down spectroscopy in the gas phase. The B_3 molecule was generated in a supersonic planar plasma containing decaborane ($B_{10}H_{14}$) and neon as a carrier gas. The rotational structure pattern is that of a cyclic molecule. It is analyzed assuming an equilateral triangle in both electronic states. The band origin is determined to be 21 853.52 cm^{-1}, and the bond lengths 1.603 77(106) Å in the ground and 1.619 07(96) Å in the excited electronic state are inferred from analysis of the rotational structure. © *2004 American Institute of Physics.*
[DOI: 10.1063/1.1791153]

I. INTRODUCTION

Well resolved absorption and emission spectra of cyclic trimers have been reported only for few species, including, Al_3,[1] Li_3,[2] Cu_3,[3] H_3^+,[4] and Na_3.[5] As the small boron molecules have applications in industry as chemical insulators, explosives, semiconductors, and high energy density materials, their structure is of relevance.[6,7] The boron trimer has been investigated only in rare gas matrices. First came the electron-spin-resonance observation which showed that B_3 contains an unpaired electron and that the three nuclei are equivalent.[8] The infrared spectrum of B_3 was also observed,[1] and recently the $2\,^2E' \leftarrow X\,^2A_1'$ electronic transition of B_3 in a neon matrix was identified using a mass selective approach.[9] However, there is no spectroscopic information on the boron trimer B_3 in the gas phase.

There is interest in the spectrum of cyclic B_3 because several of the excited electronic states are degenerate in D_{3h} symmetry. According to the Jahn-Teller theorem, there exists at least one vibrational mode that removes the electronic degeneracy and results in the stabilization of the lowest component by lowering the symmetry of the equilibrium structure. Most recent theoretical calculations on B_3 predicted an equilateral structure (D_{3h}) with an $^2A_1'$ electronic symmetry in the electronic ground state and an obtuse triangle (C_{2v}) with an apex angle $\geqslant 60°$ for the $2\,^2E'$ excited electronic state.[8,10,11] However, a low stabilization energy (difference between the conical intersection and the minima) compared with zero point energy for the $2\,^2E'$ state is reported.[9] Therefore the B_3 molecule can be considered to have D_{3h} symmetry in the $2\,^2E'$ state as an effective structure and the $2\,^2E' \leftarrow X\,^2A_1'$ electronic system can be considered as a quasi "D_{3h}-D_{3h}" transition.

In the present work we report the observation of the rotationally resolved origin band of the $2\,^2E' \leftarrow X\,^2A_1'$ electronic spectrum of B_3. The analysis of the spectrum gives an estimate of the molecular geometry; the first gas phase structural determination.

a)Author to whom correspondence should be addressed; Fax: +41-61-2673855. Electronic mail: J.P.Maier@unibas.ch

II. EXPERIMENT

This consists of a standard cavity ring down setup sampling a plasma generated in a pulsed supersonic slit jet expansion.[12] A small fraction of pulsed laser light from a tunable dye laser is coupled into an optical cavity consisting of two highly reflective mirrors ($R > 99.99\%$). The fraction of light leaking out of the cavity has an envelope which is a first-order exponential decay, $\exp(-t/\tau)$. The ring down time τ reflects the absorption coefficient. A spectrum is recorded by measuring τ as function of the wavelength of the laser (running at 30 Hz). Forty-five ring down events are averaged at each wavelength before the digitized data are downloaded to a workstation. The ~ 0.05 cm^{-1} linewidth of the laser was attained with an internal etalon.

The pulsed slit jet system is located in a vacuum chamber evacuated by a roots blower. The plasma is produced in a nozzle incorporating a discharge in the high pressure expansion. The orifice comprises a metal plate anode and two sharp stainless steel cathodes that form the actual slit (30 mm×300 μm). A pulsed negative voltage (−800 V/100 mA and 100 μs in duration) is applied. The geometry of the orifice is such that the discharge is confined upstream of the supersonic expansion. To produce B_3, solid $B_{10}H_{14}$ is heated in the oven to 70±10 °C with neon as a carrier gas at a backing pressure of 10 bars. In order to avoid condensation inside the source, the valve and body of the nozzle are heated as shown in Fig. 1. The B_3 molecules are efficiently produced at a distance 5 mm down stream from the slit. The spectrum is calibrated via the neon atomic lines that are observed in the jet expansion.

III. RESULTS

The $2\,^2E' \leftarrow X\,^2A_1'$ electronic spectrum of B_3 was initially identified in absorption in a 6 K neon matrix using mass selection with origin band located at 21 828 cm^{-1}.[9] Based on this the band was sought in the gas phase. The absorption signal was subsequently found near 21 900 cm^{-1} (Fig. 2) and the observed profile of the band, ~ 25 cm^{-1} in width, was in a good agreement with preliminary simulations. No other signal could be detected within ±300 cm^{-1}

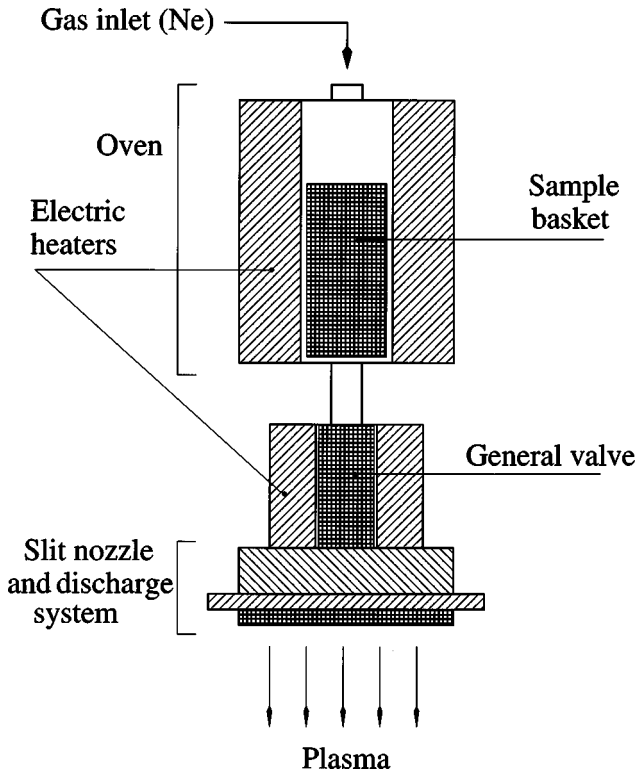

FIG. 1. Schematic diagram of the source used to produce B_3. Decaborane was heated up to 70 ± 10 °C in the oven. Neon at a backing pressure of 10 bars was used as a carrier gas. The pulsed plasma was produced by a slit nozzle to which the high voltage was applied.

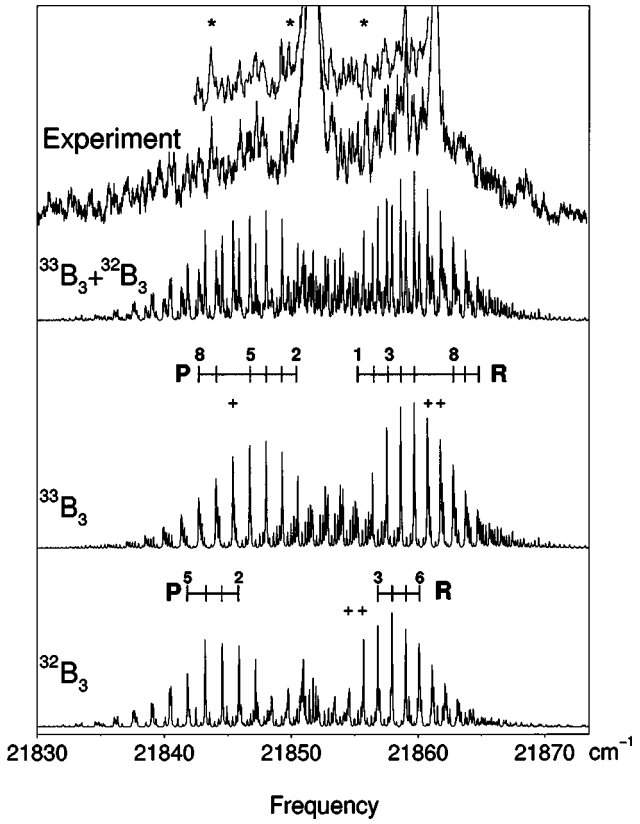

FIG. 2. Rotationally resolved $2\,^2E'\leftarrow X\,^2A_1'$ electronic origin band of B_3 in the gas phase measured by cavity ring down spectroscopy through a supersonic planar plasma. The two upper traces are independent recordings to show that the peaks are real and not noise. The three bottom traces are the simulated patterns $^{33}B_3+^{32}B_3$ (in ratio 4:3), $^{32}B_3$ and $^{33}B_3$. The two strong lines off scale belong to neon. Bands marked with* are unassigned. Lines in the simulation for which counterparts in the spectrum could not be found are marked with "+."

from the observed band. Though the spectrum visually appears "noisy" (typical S/N of at least 5) all the peaks are genuine. This is shown by the top trace which is an independent recording of this part of the band. Corresponding traces were obtained for other regions proving that all the lines given in Tables I and III are real.

The spectrum exhibits rotationally resolved P and R branches slightly blended with strong neon atomic lines. The Q branch is not visible due to a complex splitting and blending with an intense neon line. Actually, it is a composition of four spectra, as two boron isotopes are present. Because the natural isotopic abundance of ^{11}B:^{10}B in the precursor is 4:1, the relative concentration of the two isotopomers $^{33}B_3$:$^{32}B_3$ (two equivalent structures of $^{10}B^{11}B_2$) should be 4:3. The peaks in the spectra of $^{31}B_3$ and $^{30}B_3$ could not be assigned due to their small abundance. As a result, the observed spectrum is essentially an overlap of the two isotopomers $^{33}B_3$ and $^{32}B_3$.

The B_3 cyclic molecule in the excited degenerate state should undergo a deformation due to the Jahn-Teller effect, however, the distortion from an equilateral triangle can be neglected as a result of low stabilization energy [merely 39 cm^{-1} compared with a zero-point energy (1522 cm^{-1}) in the $2\,^2E''$ state[9]]. A similar situation was encountered for the cyclic C_3H radical, where deformations of the C_{2v} structure were neglected due to small energy differences between the C_s and C_{2v} forms.[13] Therefore, it is reasonable to assume that the effective symmetry of the $2\,^2E'$ state is D_{3h} for the analysis of the rotational structure in the observed spectrum.

The measured positions of the $^{33}B_3$ lines are given in Table I. The spectral line frequencies were analyzed using a conventional Hamiltonian for a symmetric top molecule. In order to analyze the imperfectly resolved rotational spectrum it was assumed that the structure of the B_3 molecule has D_{3h} symmetry in both states. This way the number of spectro-

TABLE I. Frequencies (in cm^{-1}) and assignments in the $2\,^2E'\leftarrow X\,^2A_1'$ absorption spectrum of $^{33}B_3$.

N_K	ν_{obs}	ν_{calc}	$\nu_{obs}-\nu_{calc}$
1_1-2_2	21 850.374	21 850.543	−0.169[a]
2_2-3_3	21 849.223	21 849.296	−0.073
3_3-4_4	21 848.070	21 848.027	0.043
4_4-5_5	21 846.731	21 846.736	−0.005
6_6-7_7	21 844.118	21 844.086	0.032
7_7-8_8	21 842.710	21 842.727	−0.017
1_1-0_0	21 855.230	21 855.305	−0.075
2_2-1_1	21 856.499	21 856.440	0.059
3_3-2_2	21 857.600	21 857.552	0.048
4_4-3_3	21 858.629	21 858.642	−0.013
5_5-4_4	21 859.690	21 859.710	−0.020
8_8-7_7	21 862.770	21 862.778	−0.008
9_9-8_8	21 863.713	21 863.756	−0.043
10_{10}-9_9	21 864.749	21 864.712	0.037

[a]Not included in the least-squares fit.

TABLE II. Bond lengths and spectroscopic constants of the $^{33}B_3$ molecule inferred from the partial rotational analysis of the $2\,^2E' \leftarrow X\,^2A_1'$ electronic origin band.[a]

	$^2A_1'$		$2\,^2E'$	
	Obs.	Calc.[b]	Obs.	Calc.[b]
r_0 (Å)	1.603 77(106)		1.619 07(96)	
θ_0 (deg)	60.0[c]		60.0[c]	
r_e (Å)		1.5706		1.5955
θ_e (deg)		60.0		60.8
T_{00} (cm^{-1})			21 853.52[d]	22 723
B (cm^{-1})	1.190 64(157)[e]		1.168 25(138)[e]	
C (cm^{-1})	0.595 32(79)[e]		0.584 12(69)[e]	

[a]The numbers in parentheses represent the one standard deviation derived from the least square fitting. A rms of the fitting is 0.043 cm^{-1}.
[b]Reference 9.
[c]Fixed.
[d]Error of calibration is around 0.01 cm^{-1}.
[e]The rotational constants were calculated from the determined molecular structures.

scopic parameters could be reduced to 3; the bond lengths r', r'' and band origin T_{00} were then determined directly from a least-squares fit to the line positions.

The results for the $^{33}B_3$ molecule are listed in Table II. The determined bond lengths (r_0) are 2% longer than the calculated ones (r_e) (Ref. 9) in both the ground and excited states. In the ground state this is because of zero-point vibrations as the analysis assumes a negligible inertial defect. The difference in the excited state is additionally caused by imperfections of the simple model used (assuming an equilateral triangle $\theta=60°$ and ignoring the Jahn-Teller effect) and anharmonicity of the potential.

The observed rotational profile was also simulated with the obtained molecular constants using the program WANG.[14] The simulated spectrum of $^{33}B_3$ is shown in Fig. 2. Best agreement with the experiment was attained with a rotational temperature of 30 K. A linewidth of 0.05 cm^{-1} was used for the simulation, though in the observed spectrum it is larger due to Doppler and/or lifetime broadening.

In the case of the $^{32}B_3$ isotopomer the simulation was based on the same geometry and temperature parameters as inferred for $^{33}B_3$ but using a conventional Hamiltonian of an asymmetric top molecule. It was also assumed that only the B_2-A_1 transition, which is a type, occurs. The rotational constants used for the $^{32}B_3$ molecule were $A:B:C=1.2696:1.1906:0.6144\,cm^{-1}$ for the ground, and 1.2457:1.1682:0.6029 cm^{-1} for the excited state. The spectrum of $^{32}B_3$ was then shifted by -1.94 cm^{-1} (from T_{00} of $^{33}B_3$) to get the best agreement with the observation (Fig. 2). The isotopic shift of -1.94 cm^{-1} is reasonable for an origin band.

In all, 34 rotational transitions were assigned; 14 of them are attributed to the $^{33}B_3$ molecule and the rest to $^{32}B_3$ (Table III). The presented rotational assignment and molecular structure of the B_3 molecule should be considered as tentative, because the insufficient S/N ratio of the spectrum decreases the accuracy of the molecular structure determination. Lines of $^{31}B_3$ ($\approx$19% of the $^{33}B_3$ intensity) disturb the line profiles of $^{32}B_3$ and $^{33}B_3$ transitions. There are few unassigned lines, few missing ones, and some are obscured by intense neon atomic lines (Fig. 2). However, the consistency of the whole analysis is sufficient to conclude that the observed rotationally resolved spectrum is indeed the $2\,^2E' \leftarrow X\,^2A_1'$ transition of the cyclic B_3 molecule, and leads to the first structural information in the gas phase.

TABLE III. Frequencies (in cm^{-1}) and assignments in the $2\,^2E' \leftarrow X\,^2A_1'$ absorption spectrum of $^{32}B_3$.[a]

$N_{K_aK_c}$	ν_{obs}	ν_{calc}	$\nu_{obs}-\nu_{calc}$
2_{12}-3_{13}	21 847.174	21 847.197	−0.023
2_{02}-3_{03}		21 847.183	−0.009
3_{13}-4_{14}	21 845.859	21 845.877	−0.018
3_{03}-4_{04}		21 845.876	−0.017
4_{14}-5_{15}	21 844.525	21 844.544	−0.019
4_{04}-5_{05}			
5_{15}-6_{16}	21 843.220	21 843.188	0.032
5_{05}-6_{06}			
6_{16}-7_{17}	21 841.821	21 841.809	0.012
6_{06}-7_{07}			
7_{17}-8_{18}	21 840.420	21 840.407	0.013
7_{07}-8_{08}			
4_{14}-3_{13}	21 856.843	21 856.832	0.011
4_{04}-3_{03}		21 856.833	0.010
5_{15}-4_{14}	21 857.952	21 857.934	0.018
5_{05}-4_{04}			
6_{16}-5_{15}	21 859.041	21 859.013	0.028
6_{06}-5_{05}			
7_{17}-6_{16}	21 860.125	21 860.068	0.057
7_{07}-6_{06}			

[a]The assignment and calculated frequencies were derived on the assumption that the bond lengths of $^{32}B_3$ and $^{33}B_3$ are equal, and the isotopic shift is -1.94 cm^{-1}.

ACKNOWLEDGMENTS

This work has been supported by the Office of Aerospace Research and Development and the Swiss National Science Foundation (Project No. 200020-100019).

[1] S. Li, R. J. Van Zee, and W. Weltner, Chem. Phys. Lett. **262**, 298 (1996).
[2] M. Keil, H.-G. Kraemer, A. Kudell, M. A. Baig, J. Zhu, W. Demtroeder, and W. Meyer, J. Chem. Phys. **113**, 7414 (2000).
[3] A. O'Keffe, J. J. Scherer, A. L. Cooksy, R. Sheeks, J. Heath, and R. J. Saykally, Chem. Phys. Lett. **172**, 214 (1990).
[4] A. R. W. McKellar and J. K. G. Watson, J. Mol. Spectrosc. **191**, 215 (1998).
[5] H. A. Eckel, J. M. Gress, J. Biele, and W. Demtroeder, J. Chem. Phys. **98**, 135 (1993).
[6] L. Hanley, J. L. Whitten, and S. L. Anderson, J. Phys. Chem. **92**, 5803 (1988).
[7] J. D. Presilla-Marquez, C. W. Larson, and P. G. Carrick, J. Chem. Phys. **105**, 3398 (1996).
[8] Y. M. Hamrick, R. J. Van Zee, and W. Weltner, J. Chem. Phys. **96**, 1767 (1992).
[9] M. Wyss, E. Riaplov, A. Batalov, J. P. Maier, T. Weber, W. Meyer, and P. Rosmus, J. Chem. Phys. **119**, 9703 (2003).
[10] R. Hernandez and J. Simons, J. Chem. Phys. **94**, 2961 (1991).
[11] J. M. L. Martin, J. P. Francois, and R. Gijbels, J. Chem. Phys. **90**, 6469 (1989).
[12] H. Linnartz, T. Motylewski, and J. P. Maier, J. Chem. Phys. **109**, 3819 (1998).
[13] S. Yamamoto and S. Saito, J. Chem. Phys. **101**, 5484 (1994).
[14] D. Luckhaus and M. Quack, Mol. Phys. **63**, 745 (1989).

Available online at www.sciencedirect.com
SCIENCE DIRECT®
Chemical Physics Letters 404 (2005) 315–317
CHEMICAL PHYSICS LETTERS
www.elsevier.com/locate/cplett

The near infrared $1\,^2A_2'' \leftarrow X\,^2A_1'$ electronic transition of B_3 in a neon matrix

Anton Batalov, Jan Fulara [1], Ivan Shnitko, John P. Maier *

Department of Chemistry, University of Basel, Klingelbergstrasse 80, CH-4056 Basel, Switzerland

Received 9 January 2005

Abstract

The $1\,^2A_2'' \leftarrow X^2A_1'$ electronic transition of the B_3 molecule with origin band at 5990 cm^{-1} has been observed in a 6 K neon matrix. A vibrational progression in the spectrum corresponds to the excitation of the $\nu_1(a_1')$ vibrational mode in the $1\,^2A_2''$ state with a frequency of ~1092 cm^{-1}. The band system was detected after laser ablation of a boron rod and the origin band also after mass-selected deposition of B_3^- anions with subsequent neutralization.

1. Introduction

Structure and properties of boron clusters are interesting for fundamental science. Boron is the only element except carbon that can build molecules of any size by covalent bonds, and there are a number of applications [1,2]. Nevertheless, even molecules as small as B_3 are spectroscopically not thoroughly investigated. The first study of B_3 was by ESR [3] followed by IR spectroscopy [4] both in rare gas matrices. A previous publication reported the $1\,^2E' \leftarrow X^2A_1'$ and $2\,^2E' \leftarrow X^2A_1'$ electronic transitions of B_3 in a 6 K neon matrix [5]. The rotationally resolved origin band of the $2\,^2E' \leftarrow X^2A_1'$ transition has been measured since then in absorption in the gas phase and analyzed [6]. Ab initio calculations on the ground and excited electronic states of B_3 are available [5,7]. In the present work the $1\,^2A_2'' \leftarrow X^2A_1'$ electronic transition of B_3 has been observed for the first time in a 6 K neon matrix.

2. Experimental

The main features of the experimental set up have been described [8]. Two approaches were used to produce boron clusters: one with a cesium sputter ion source and the other by laser ablation. Boron rod (99.6% purity) with a natural isotopic composition was used as a target for the laser vaporization. B_4C, LaB_6 and BN rods were used as well.

A slowly rotating sample rod was installed ~10 cm from the matrix substrate. A 532-nm pulsed Yag laser beam, ~20 mJ, 20 Hz, was focused on the rod. A mixture of ionic and neutral ablation products was co-deposited with excess of neon (or argon) onto a sapphire substrate coated with rhodium and cooled to a temperature of 6 K. Spectra in the 1100–12 000 cm^{-1} range were recorded after sampling the neon matrix by a Fourier transform spectrometer applying a double reflection technique. The light beam reflects from the metal surface of the substrate on which the neon matrix sits, then from a mirror into the matrix again and back from the substrate. Absorption spectra in the 220–1100 nm region have been measured by passing monochromatic light through the matrix in a wave-guide manner [9].

* Corresponding author. Fax +41 61 267 38 55.
E-mail address: j.p.maier@unibas.ch (J.P. Maier).
[1] Permanent address: Institute of Physics, Polish Academy of Sciences, Al.Lotnikow 32-46, Pl-02668 Warsaw, Poland.

0009-2614/$ - see front matter © 2005 Elsevier B.V. All rights reserved.
doi:10.1016/j.cplett.2005.01.081

In order to assign the observed band system, experiments with mass-selected boron anions, produced in a cesium sputter source [10] have been carried out. The anions produced in the source were guided by means of electrostatic lenses into the quadrupole mass filter and were separated from neutral molecules by deflecting the beam through 90°. The B_3^- ions were mass selected and co-deposited with excess of neon to form a matrix at ~6 K. A typical current of B_3^- impinging on the matrix was ~5 nA. This technique allowed the deposition of B_3^- exclusively but it was not possible to obtain a high concentration of neutral B_3 in the matrix.

Neutral B_3 was produced by irradiation of the matrix with a mercury medium pressure lamp during ~30 min. An important procedure was annealing up to 8.5 K making the neon matrix softer and thus allowing relaxation of the trapped molecules to their energetic minima (and even some reactions to proceed).

3. Observations

Several new bands were seen after laser vaporization of the boron rod in the infrared (Fig. 1), in addition to the previously reported $1^2E' \leftarrow X^2A_1'$ and $2^2E' \leftarrow X^2A_1'$ absorption systems of the B_3 molecule [5,6] and those of the B and B_2 species [11–13] in the visible and UV. The new system comprises three peaks, separated by ~1092 cm^{-1}, with origin band at 5990 cm^{-1} (Table 1). This was seen after vaporization of B_4C and LaB_6 rods as well. The intensity of the bands increases after irradiation of the matrix with UV photons indicating a neutralization process. Thus one can conclude that the carrier is a neutral boron molecule. The band system is not likely due to a boron and hydrogen (common impurity) containing species. When 1% of hydrogen was introduced into the matrix (Ne/H_2 ratio of 100/1) the intensity of bands remained the same. The absorption band at 6268 cm^{-1} (marked with *) is due to an unknown impurity. Its intensity depended on the rod used.

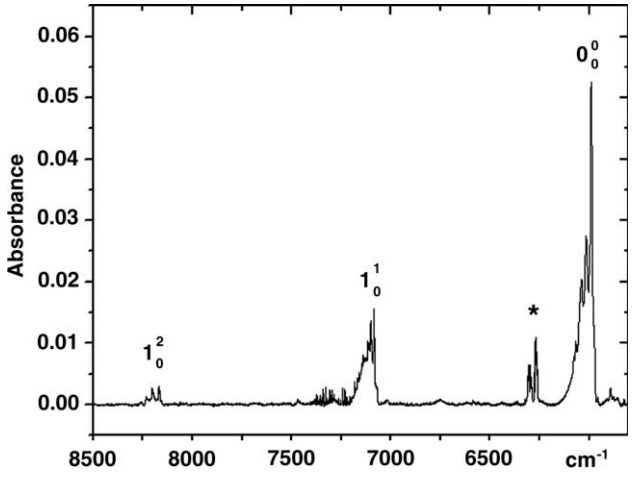

Fig. 1. The $1^2A_2'' \leftarrow X^2A_1'$ electronic absorption spectrum of B_3 in a 6 K neon matrix after laser vaporization of a pure boron rod. The band marked with * is due to an unknown impurity.

Table 1
Positions of the band maxima (±0.2 cm^{-1}) in the $1^2A_2'' \leftarrow X^2A_1'$ electronic transition of B_3 in a 6 K neon matrix

ν (cm^{-1})	$\Delta\nu$ (cm^{-1})	Vibrational transition
5990	0	0_0^0
7085	1095	1_0^1
8169	2179	1_0^2

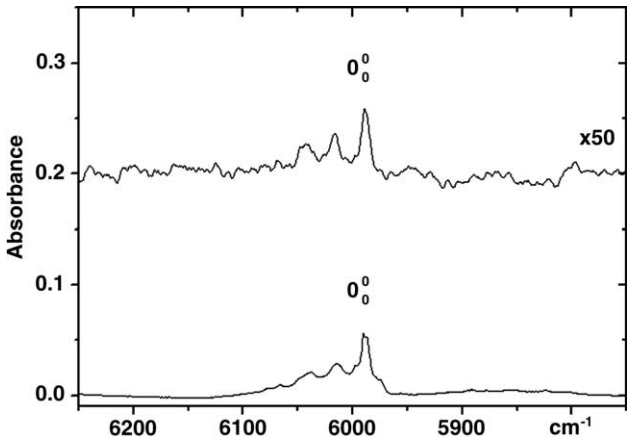

Fig. 2. The origin band of the $1^2A_2'' \leftarrow X^2A_1'$ electronic absorption of B_3 in a 6 K neon matrix after laser vaporization of a pure boron rod (lower trace), and after mass-selected deposition of B_3^- with subsequent neutralization by UV irradiation (upper trace – multiplied by a factor of 50 and smoothed).

Fine structure of the bands is due to matrix site effects. The trapped molecules have different orientations in the neon lattice. One can see that the three bands of the new system possess the same structure. After annealing to 8.5 K intensity redistribution is observed. The site-pattern is different when argon is used as the matrix.

Mass selected deposition of B_3^- followed by neutralization led also to the appearance of the 5990 cm^{-1} absorption band (Fig. 2). The wavelength of the band and the site structure are exactly the same as in the laser vaporization spectrum. However, the intensity is about 50 times lower for the mass selected case. The bands at 7085 and 8169 cm^{-1} corresponding to vibrational excitation in the upper electronic state were not observed in the mass-selected experiment due to a low signal to noise ratio. It is concluded that the observed system with the origin band at 5990 cm^{-1} is an electronic transition of B_3.

4. Discussion

It is theoretically established that B_3 has an equilateral triangle structure (D_{3h} group) with $^2A_1'$ symmetry in the ground state with electronic configuration $(1a_1')^2(1e')^4(1a_2'')^2(2a_1')^1$ [5,7,14]. The only excited states accessible from the ground state by electric dipole transitions are $^2A_2''$ and $^2E'$. The electronic transitions $1\,^2E' \leftarrow X\,^2A_1'$ and $2\,^2E' \leftarrow X\,^2A_1'$ of B_3 in a neon matrix have been studied earlier [5]. The ab initio calculations predict that the transition to the lowest excited state with $^2A_2''$ symmetry lies at $\sim$6300 cm^{-1}; in an earlier calculation 7000 cm^{-1} was obtained [7]. These are energetically in good agreement with the observed origin band (Fig. 1). Consequently the new absorption system is assigned to the $1\,^2A_2'' \leftarrow X\,^2A_1'$ dipole-allowed electronic transition of B_3.

B_3^- has been studied by photoelectron spectroscopy [14] giving the vertical detachment energies of 2.82 and 3.56 eV to the B_3 final states $X\,^2A_1'$ and $1\,^2A_2''$. The 0.74 eV ($\sim$6000 cm^{-1}) difference between these is also in agreement with the present observations.

Equilateral triangular B_3 molecule has two normal vibrations: a_1' and e'. Only transitions to the totally symmetric vibrational levels of the upper state ($1\,^2A_2''$) are allowed from the $X\,^2A_1'$ ground state, the solely populated level at 6 K. Hence the bands at 7085 and 8169 cm^{-1} (Table 1) are assigned as the first two members of the progression structure associated with the a_1' normal mode excitation in the upper $1\,^2A_2''$ state. The $\nu_1(a_1')$ frequency is thus inferred to be 1092 ± 3 cm^{-1}, in agreement with the analysis of the photoelectron spectrum [14] of B_3^- which yielded the value 1130 ± 30 cm^{-1}.

Acknowledgments

This study was supported by the Office of Aerospace Research and Development and the Swiss National Science Foundation (Project 200020-100019/1).

References

[1] R.N. Grimes, J. Chem. Ed. 81 (2004) 658.
[2] L.H. Hanley, J.L. Whitten, S.L. Anderson, J. Am. Chem. Soc. 92 (1988) 5803.
[3] Y.M. Hamrick, R.J. Van Zee, W.J. Weltner, J. Chem. Phys. 96 (1992) 1767.
[4] S. Li, R.J. Van Zee, W.J. Weltner, Chem. Phys. Lett. 262 (1996) 298.
[5] M. Wyss, E. Riaplov, A. Batalov, J.P. Maier, T. Weber, W. Meyer, P. Rosmus, J. Chem. Phys. 119 (2003) 9703.
[6] P. Cias, M. Araki, A. Denisov, J.P. Maier, J. Chem. Phys. 121 (2004) 6776.
[7] R. Hernandez, J. Simons, J. Chem. Phys. 94 (1991) 2961.
[8] J.P. Maier, Chem. Soc. Rev. 26 (1997) 21.
[9] V.E. Bondybey, T.J. Sears, J.H. English, T.A. Miller, J. Chem. Phys. 73 (1980) 2063.
[10] D. Forney, J. Fulara, P. Freivogel, M. Jakobi, D. Lessen, J. Chem. Phys. 103 (1995) 48.
[11] W.R.M. Graham, W. Weltner, J. Chem. Phys. 65 (1976) 1516.
[12] S. Tam, M. Macler, M.E. DeRose, M.E. Fajardo, J. Chem. Phys. 113 (2000) 9067.
[13] P.J. Bruna, J.S. Wright, J. Phys. B: At. Mol. Opt. Phys. 23 (1990) 2197S.
[14] H.-J. Zhai, L.-S. Wang, A.N. Alexandrova, A.I. Boldyrev, V.G. Zakrzewski, J. Phys. Chem. A 107 (2003) 9319.

Vibrations in the B_4 rhombic structure

Roberto Linguerri, Isabelle Navizet, and Pavel Rosmus
Laboratoire de Chimie Théorique, Université de Marne la Vallée, F-77454 Champs sur Marne, France

Stuart Carter
Department of Chemistry, University of Reading, Reading RG6 2AD, United Kingdom

John P. Maier
Department of Chemistry, University of Basel, Klingelbergstrasse 80 CH-4056 Basel, Switzerland

(Received 12 July 2004; accepted 12 October 2004; published online 28 December 2004)

A double minimum six-dimensional potential energy surface (PES) is determined in symmetry coordinates for the most stable rhombic (D_{2h}) B_4 isomer in its ^1A_g electronic ground state by fitting to energies calculated *ab initio*. The PES exhibits a barrier to the D_{4h} square structure of 255 cm^{-1}. The vibrational levels ($J=0$) are calculated variationally using an approach which involves the Watson kinetic energy operator expressed in normal coordinates. The pattern of about 65 vibrational levels up to 1600 cm^{-1} for all stable isotopomers is analyzed. Analogous to the inversion in ammonia-like molecules, the rhombus rearrangements lead to splittings of the vibrational levels. In B_4 it is the B_{1g} (D_{4h}) mode which distorts the square molecule to its planar rhombic form. The anharmonic fundamental vibrational transitions of $^{11}B_4$ are calculated to be (splittings in parentheses): $G(0)=2352(22)$ cm^{-1}, $\nu_1(A_{1g})=1136(24)$ cm^{-1}, $\nu_2(B_{1g})=209(144)$ cm^{-1}, $\nu_3(B_{2g})=1198(19)$ cm^{-1}, $\nu_4(B_{2u})=271(24)$ cm^{-1}, and $\nu_5(E_u)=1030(166)$ cm^{-1} (D_{4h} notation). Their variations in all stable isotopomers were investigated. Due to the presence of strong anharmonic resonances between the B_{1g} in-plane distortion and the B_{2u} out-of-plane bending modes, the higher overtones and combination levels are difficult to assign unequivocally. © *2005 American Institute of Physics.* [DOI: 10.1063/1.1828045]

I. INTRODUCTION

Boron catenation leads to a large variety of stable structures which are of interest in many research areas and applications.[1] They have been the subject of numerous experimental[2–9] and theoretical[10–28] investigations.

Spectral data are still limited for pure boron clusters. Two electronic transitions of the B_2 molecule have been observed in the gas phase[8] and in cold matrices.[9] Recently, the electronic absorption spectra of B_3 and B_3^- in Ne matrix,[29] and the gas phase photoelectron spectra[30] of B_3^- and B_4^- were reported.

The present work deals with the *ab initio* calculations of the low lying vibrational levels in the most stable rhombic B_4 isomer in its $X\,^1A_g$ ground state. In previous theoretical studies[10–12,22–28,30] the equilibrium structures[11,12,22–25,28,30] and harmonic wave numbers[25,26,30] were calculated for the D_{2h} rhombic minimum or for the square D_{4h} transition state. However, the computations of a realistic pattern of vibrational levels in B_4 require methods going beyond the harmonic approximation. The existence of two equivalent minima (there are six equivalent ones if permutations including bond breaking are considered to be feasible symmetry operations) leads to splittings and additional complications for the vibrational assignments are caused by the presence of strong low lying anharmonic resonances.

In the tetraatomic cyclic clusters, the lower symmetry minima can correlate with electronically degenerate states of higher symmetry forming Jahn–Teller pairs. In fact, the theory for this type of Born–Oppenheimer breakdown has been originally formulated for the X_4 planar molecules.[31,32] Based on the model of Pearson,[33] the planar rhombic equilibrium structures have been considered in previous theoretical studies (for instance, in Ref. 25) as a result of the second-order (pseudo) Jahn–Teller effect. The coupling of at least two electronic states is supposed to lead to the D_{2h} rhomboid minimum. The archetypical example[33] of the pseudo-Jahn–Teller effect is the ammonia-like D_{3h}/C_{3v} structure, in which the ground and the first excited singlet states are coupled by the inversion mode. Recent calculations clearly showed that the near-equilibrium vibrational problem can be solved very accurately within the Born–Oppenheimer approximation.[34–36] In B_4 the coupling is via the B_{1g} mode, which distorts the square molecule to its planar rhombic $X\,^1A_g$ form. Like in ammonia, the first electronically excited singlet state in B_4 is energetically well separated from the ground state. We have calculated the vertical excitation energy to the $A\,^1B_{1g}$ state at 3.1 eV above the rhombic equilibrium and 3.3 eV above the square barrier (cf. following section). In the photodetachment electron spectra of B_4^- (Ref. 30) only excited triplet states were detected, lying between 1 and 2.4 eV above the $X\,^1A_g$ ground state. The excited singlet states were calculated at higher energies.[30] On the electronic ground state potential energy surface (PES) the next higher isomer having C_{2v} symmetry has been calculated to lie at 1.77 eV,[11] or 2.33 eV[12] with a barrier on the isomerization path of 0.43 eV[12] above the rhombic structure. Therefore, for the energy region of the fundamental vibrational transitions a single adiabatic PES with two equivalent minima is consid-

TABLE I. Definition of the symmetry relations of the planar structures used in the assignments.

Mode	D_{4h} $^{10}B_4, ^{11}B_4$	D_{2h}[a] $^{10}B_2{}^{11}B_2$	C_{2v}[b] $^{10}B^{11}B_3, ^{11}B^{10}B_3$	C_{2v}[b] $^{10}B_2{}^{11}B_2$	C_s
1	A_{1g}	A_g	A_1	A_1	A'
2	B_{1g}	A_g	A_1	B_2	A'
3	B_{2g}	B_{1g}	B_2	A_1	A'
4	B_{2u}	B_{1u}	B_1	A_2	A''
5	E_u	$B_{2u}+B_{3u}$	A_1+B_2	A_1+B_2	$2A'$

[a]z axis is perpendicular to the $\sigma(xy)$ molecular plane.
[b]C_2 lies in the z axis and $\sigma(yz)$ is the molecular plane.

ered to be a sufficiently good approximation.

Similar rhombus/square PES topology has been predicted in electronic ground and excited states of numerous X_4 clusters, for instance, in Li_4,[37,38] C_4,[39] or Au_4.[40,41] Interestingly, in Si_3C two distinct rhombic planar structures were detected experimentally[42] and one of the isomers in interstellar space.[42]

The nuclear motion problem has been solved by the MULTIMODE approach.[43] It has been demonstrated that MULTIMODE can deliver a near-exact set of vibrational energies for molecules such as ammonia,[44] where tunneling through a potential barrier is experienced. Using the same PES, identical variational results were obtained with MULTIMODE with the full Hamiltonian in internal coordinates[45] and with the reaction path Hamiltonian.[46] The MULTIMODE method requires a stationary point at which a normal mode analysis is performed. The obvious choice for ammonia, where tunneling splittings were of interest, was the inversion saddle point of D_{3h} symmetry. Similarly, for B_4, the square D_{4h} saddle point is used to obtain the normal modes required for the variational calculations of the anharmonic wave functions.

II. COMPUTATIONAL APPROACH

All electronic structure calculations were carried out using the MOLPRO program.[47] The valence electronic configuration of the B_4 electronic ground state $X\,^1A_g(D_{2h})$ is $1a_g^2 1b_{2u}^2 1b_{3u}^2 1b_{1u}^2 1b_{1g}^2 2a_g^2$. Because it dominates the configuration expansion in the region near the D_{4h} barrier and at the minimum D_{2h} structure, we used the coupled cluster with perturbative triples (CCSD(T)) method[48] and the correlation-consistent polarized valence quadruple zeta basis set (cc-pVQZ) of Dunning[49] to calculate the 643 energies used in the analytical fit. The core and core-valence electron correlation was neglected. The vertical excitation energy of the first electronically excited $A\,^1B_{1g}$ state at the optimized rhombic equilibrium structure (cf. following section) has been calculated to be 3.12 eV equation of motion-coupled clusters (EOM-CC);[50] cc-pVQZ basis set[49] and 2.92 eV full valence complete active space self-consistent field (CASSCF),[51] aug-cc-pVTZ basis set[49], for the square structure 3.35 eV (EOM-CC) and 3.82 eV (full valence CASSCF). As we have performed calculations for all six stable isotopomers of B_4 we define for clarity the symmetry relations between different point groups used. In Table I the definition of axis, planes, and corresponding irreducible representations are given. After having tested various types of

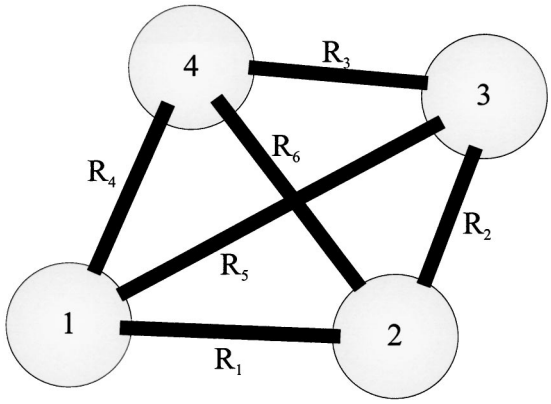

FIG. 1. Nuclear distances employed in the definition of the symmetry coordinates.

coordinates the best six-dimensional fit was obtained with the following D_{2h} symmetry-adapted coordinates (see Fig. 1 for the definition of the distances):

$$S_{1_{A_g}} = \tfrac{1}{2}(\Delta R_1 + \Delta R_2 + \Delta R_3 + \Delta R_4),$$

$$S_{2_{B_{1g}}} = \tfrac{1}{2}(\Delta R_1 - \Delta R_2 + \Delta R_3 - \Delta R_4),$$

$$S_{3_{B_{2u}}} = \tfrac{1}{2}(\Delta R_1 - \Delta R_2 - \Delta R_3 + \Delta R_4),$$

$$S_{4_{B_{3u}}} = \tfrac{1}{2}(\Delta R_1 + \Delta R_2 - \Delta R_3 - \Delta R_4),$$

$$S_{5_{A_g}} = \frac{1}{\sqrt{2}}(\Delta R_5 - \Delta R_6),$$

$$S_{6_{B_{1u}}} = \Delta\tau,$$

τ being the dihedral angle between the planes B_1-B_2-B_3 and B_2-B_3-B_4. The following polynomial expansion is used to represent the six-dimensional double minimum PES:

$$V(S_1,S_2,\ldots,S_6) = \sum_{i,j,k,l,m,n=0}^{4} C_{i,j,k,l,m,n} S_1^i S_2^j S_3^k S_4^l S_5^m S_6^n.$$

In the expansion only the totally symmetric products with $i+j+k+l+m \leqslant 4$ were retained. In the planar square reference geometry $R_i^0 = 2.8986$ bohrs $(i=1,4)$, $R_j^0 = 2.8986 \times \sqrt{2}$ bohr $(j=5,6)$, and $\tau^0 = 0$. The following relation including permutations of the coordinates holds: $V(S_1,S_2,S_3,S_4,S_5,S_6) = V(S_1,S_2,-S_4,-S_3,-S_5,-S_6)$. The goal was to obtain a PES valid close to the minimum and the barrier. The analytic form of the double minimum PES is available from the data base.[52]

In Fig. 2 contour plots are displayed for some typical cuts of the PES. The units on the axis are bohr for the distances and degree for the S_6 coordinate. For a given pair of coordinates all the others are fixed at the optimized geometry of the square transition state (cf. Table II). The two-dimensional cut of the S_4 versus S_3 coordinates shows an isotropic form. In fact, due to the totally symmetric products in the expansion and the aforementioned symmetry relation, the cut must be symmetric with respect to $S_3 = -S_4$ and $S_3 = S_4$ coordinate permutations. The second cut, S_6 versus S_1,

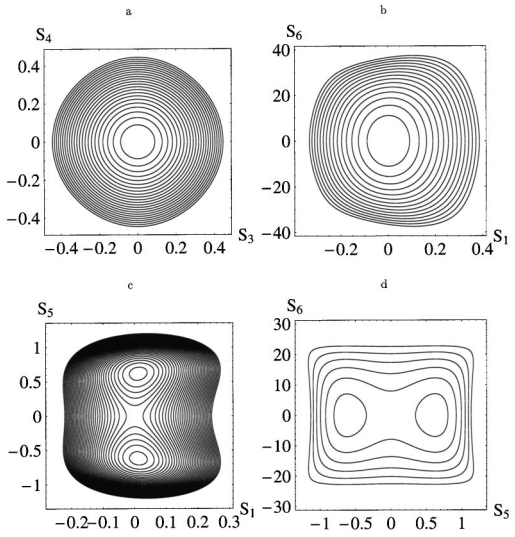

FIG. 2. Four contour plots of the double minimum six-dimensional PES of the B_4 rhombic cluster in symmetry coordinates. The distance is in bohr and angle in degree. Contour a: energy range 6000 cm^{-1}, contour step 250 cm^{-1}. Contour b: energy range 4000 cm^{-1}, contour step 250 cm^{-1}. Contour c: energy range 2000 cm^{-1}, contour step 50 cm^{-1}. Contour d: energy range 1750 cm^{-1}, contour step 250 cm^{-1}.

displays the potential for all in-plane ($S_6=0$) and out-of-plane ($S_6\neq 0$) geometries, in which $R_1=R_2=R_3=R_4$ and $R_5=R_6$. The S_5 versus S_1 cut, including the rhombic minima, gives information on how the equal sides of the tetragon ($S_2=S_3=S_4=0$) become larger when passing from the square to the rhombic structure (the S_1 value is positive for the rhombic minimum and zero for the square structure). The S_6 versus S_5 cut in the last diagram shows the change of the energy barrier with increasing out-of-plane angle, for squeezing a tetragon with $R_1=R_2=R_3=R_4=R_i^0$.

The barrier height (on the adiabatic PES) relative to the rhombic minimum has been calculated to be 255 cm^{-1}. Previously Martin *et al.*[25] reported 178 cm^{-1} ($G1$ corrected value), Zhai *et al.*[30] 283 cm^{-1} (B3LYP), and Kato and Tanaka[26] 1014 cm^{-1} (MP4).

The analysis of the PES indicates that the path corresponding to two clockwise and two anticlockwise in-phase nuclear in-plane rotations for the $r\cos(\theta)$ coordinate with $r=(d_1-d_2)/4$, and d_1 being the long and d_2 the short diagonal of the rhombus, represents a good approximation for the periodic B_{1g} ring distortion. However, there is no path connecting the two rhombic minima below the square transition state.

The PES described above was used in vibrational variational calculations with the code MULTIMODE.[53] This procedure utilizes the exact Watson kinetic energy operator in normal coordinates,[54] and therefore some suitable reference structure at which the $3N-6$ normal vibrations are defined must be first located. In order to be even handed about the two equivalent minima on the PES, the choice for such a reference structure is that of the square-planar transition state. The normal mode vectors at the transition state can then be readily specified in terms of the irreducible representations of the symmetry point group for any chosen isotopomer. However, due to the specific difficulties in employing C_{2v} symmetry (the highest currently available in MULTIMODE) for molecules with E modes in the D_{4h} point group, all we can do is to use the reflection operation in order to symmetry block the configuration interaction (CI) matrix; we therefore work in C_s symmetry throughout (two blocks A' and A''), and use the vector symmetries in order to reclassify the energy levels into irreducible representations of the point group of the transition state. The great advantage of the MULTIMODE approach in the application to the B_4 problem is the possibility to designate the anharmonic vibrational states in terms of linear combinations of vibrational configurations with harmonic quantum numbers. This is a universal bonus gained from using normal coordinates and has been the method of choice for spectroscopists for many years.

The methodology adopted in the MULTIMODE approach has been fully described on a number of occasions (see Ref. 53 and references therein). We therefore only outline the basic features relevant to this work. The initial step in the procedure is to optimize a set of 36 harmonic-oscillator primi-

TABLE II. Optimized geometries (diagonal distances) and the harmonic wave numbers of the fundamental vibrational transition in the electronic ground states of B_4.

			B_4 rhombus (D_{2h})			B_4 square (D_{4h})		
			This work[a]	b	c		This work[a]	b
Diagonals			4.591	4.703	4.659		4.100	4.126
(bohr)			3.574	3.520	3.601			
Modes	ω_1	A_g	1142	1118	1112	A_{1g}	1143	1136
(cm^{-1})	ω_2	A_g	311	433	336	B_{1g}	209i	330i
	ω_3	B_{1g}	1216	1161	1173	B_{2g}	1240	1195
	ω_4	B_{1u}	304	332	287	B_{2u}	272	238
	ω_5	B_{2u}	1013	970	966	E_u	1148	1138
	ω_5	B_{3u}	1235	1251	1201	E_u	1148	1138

[a]The harmonic wave numbers were calculated with the relative atomic mass of 10.810 for boron; cc-pVQZ basis was used (Ref. 49), the CCSD(T) total energies at the rhombic and square structures were calculated to be −98.908 391 a.u. and −98.907 260 a.u. The standard MOLPRO convergency criteria for the gradients and energies were used.
[b]MP2 approach/6-311G*; no relative mass of B was given (Ref. 25).
[c]RCCSD(T)/6-311+G*, $E_{min}=-98.839\,444$ a.u.; no relative mass of B was given (Ref. 30).

tive basis functions (NBF) for $3N-7$ normal modes by using effective one-dimensional cuts in the PES relative to the ''squeezing'' mode. These one-dimensional potentials are then used in variational calculations with the equivalent one-dimensional Hamiltonians, respectively, for which ten converged subsets (NVF) are retained for subsequent use. The raw one-dimensional, double-minimum cut is used for the squeezing mode itself (NBF=46, NVF=15), in order to optimize the corresponding harmonic-oscillator basis. The primitive harmonic-oscillator basis is defined by the values of ω arising from the Wilson FG normal mode analysis, with the exception of that for the squeezing mode, whose eigenvalue is imaginary at the planar transition state. In this case pilot calculations are carried out with various values of ω assigned to the harmonic-oscillator basis, until an optimum value is obtained which spans sufficiently into the high-energy regions of the one-dimensional cut. Providing that a sufficient number of primitive harmonic-oscillator functions are used, fully converged one-dimensional expansion functions can be obtained for modes with such gross anharmonicity. This optimization procedure is carried out using Gauss-hermite numerical quadrature involving quadrature points to integrate all matrix elements (50 for the $3N-7$ normal modes and 60 for the squeezing mode), and the resulting contracted expansion functions are then used to reduce the integration points via the HEG algorithm.[55]

The optimized one-dimensional expansion set is now used in a vibrational self-consistent-field procedure for the zero-point level. Integration of the matrix elements takes place in a series of steps ($\leqslant 5$), during which the overcounting of each M-mode potential resulting from $M+1$-mode cuts (and so on) is taken into account.[43] Likewise, integration of the Coriolis terms which involve the inverse moment-of-inertia tensor μ is performed in an analogous way. For each M-mode cut in the PES and μ, the equivalent M-mode Hamiltonian is adopted. The result of this analysis is an improved one-dimensional expansion set in the NVF basis for each of the $3N-6$ modes, and these are now used in a final CI calculation to determine the vibrational energies. The CI matrix itself is constructed by imposing a maximum quantum for each mode, together with a maximum sum-over-quanta for all modes, in a series of M-mode blocks ($M \leqslant 5$). The complete CI matrix is the total of all such blocks.[53] Finally, the resulting CI matrix is split into A' and A'' symmetry blocks. As with all variational calculations, increased CI matrices are diagonalized until the required convergence is reached. In MULTIMODE calculations, a further convergence criterion is required, and that is for the M-mode integration procedure. In this study, virtually total convergence in all levels was achieved for $M=5$, and this therefore removes the inherent approximation from the calculations.

III. RESULTS AND DISCUSSION

The computational approach used for the generation of the six-dimensional PES yielded the following spectroscopic constants for the $^{11}B_2\ X\ ^3\Sigma_g^-$ state: $R_e=1.593$ Å, $\omega_e=1048\ \mathrm{cm}^{-1}$, and $\omega_e x_e=8.92\ \mathrm{cm}^{-1}$. The corresponding experimental values[8] are $R_e=1.590$ Å, $\omega_e=1051.3\ \mathrm{cm}^{-1}$, and $\omega_e x_e=9.35\ \mathrm{cm}^{-1}$. It is difficult to estimate the accuracy of the fundamental transitions evaluated from the six-dimensional PES of B_4, but we expect to have obtained similarly reliable results. The CCSD(T) geometries and harmonic wave numbers for the minimum and the saddle point of B_4 are compared with previous theoretical data in Table II. The similarity of the $B-B$ equilibrium distances in B_2 and B_4 is related to the covalent character of the bonds in the cluster. For D_{4h} structures only one imaginary wave number is calculated for the B_{1g} mode, which transforms the square transition state to the rhombic minimum. Our optimized diagonal distances and harmonic wave numbers for B_4 differ from those calculated previously. The present results are seen to be more accurate due to the better quality of the electronic structure calculations.

The CCSD(T) values for the ω_2 ring in-plane distortion and the ω_4 ring out-of-plane bending are calculated to be almost identical. This implies that overtones or combination levels with even vibrational quanta will form anharmonic resonances considerably complicating the splitting patterns and assignments. Within a given symmetry block other nearby states interact as well.

In nature there are two stable boron isotopes, ^{10}B (abundance 19.9%) and ^{11}B (80.1%), which give rise to six different isotopomers of B_4 belonging to different point groups. The MULTIMODE calculations were all done using C_s symmetry with the plane in which the four boron atoms lie at the transition state, defining the symmetry plane. In all six isotopomers the vibrational states in Table III are assigned with the highest possible symmetries of the transition states. In the first column the consecutive numbering of all levels is used and the labels l (lower) and u (upper) indicate the split pairs. In the second column the harmonic vibrational configurations (with coefficients larger than 0.3 in the configuration expansion) are given for $^{11}B_4$. The mode numbering is defined in Table I. The results are presented in two blocks—Table III for A' symmetry and Table IV for A'' symmetry. All calculated levels for $^{11}B_4$ up to about 1500 cm^{-1} are displayed in Fig. 3, with assignments using the irreducible representations of the D_{4h} point group. Each state is designated by specifying the dominating harmonic configurations in the total wave function expansion. The zero-point energies are given relative to the electronic energy of the transition state and vary up to 122 cm^{-1} for different isotopomers. The vibrational mode splittings were deduced from the assignments in Tables III and IV. The anharmonic fundamental vibrational levels of $^{11}B_4$ are calculated to be (splittings in parentheses): $G(0)=2352(22)\ \mathrm{cm}^{-1}$, $\nu_1(A_{1g})=1136(24)\ \mathrm{cm}^{-1}$, $\nu_2(B_{1g})=209(144)\ \mathrm{cm}^{-1}$, $\nu_3(B_{2g})=1198(19)\ \mathrm{cm}^{-1}$, $\nu_4(B_{2u})=271(24)\ \mathrm{cm}^{-1}$, and $\nu_5(E_u)=1030(166)\ \mathrm{cm}^{-1}$. The corresponding values for the second abundant $^{10}B^{11}B_3$ isotopomer are 2364 (23), 1148 (24), 212 (148), 1218 (21), 274 (25), and 1041, 1042 (158,160) (all values in cm^{-1}). All IR or Raman allowed fundamentals of these two isotopomers will be clearly discernible in their spectra. According to the splittings in the ground state of about 22–26 cm^{-1} the rhombus will rearrange within about 0.75 ps, and at room temperature, because the B_{1g} and

TABLE III. Vibrational pattern in the B_4 isotopomers (A' symmetry).

Abundance (%)		$^{11}B_4$ 41.2		$^{10}B^{11}B_3$ 40.9		$^{10}B_2{}^{11}B_2$ 10.2		$^{10}B_2{}^{11}B_2$ 5.1		$^{10}B_3{}^{11}B$ 2.5		$^{10}B_4$ 0.2	
Assignment[a]		D_{4h}		C_{2v}		C_{2v}		D_{2h}		C_{2v}		D_{4h}	
0^l	$G(0)$	A_{1g}	2332.76	A_1	2363.60	A_1	2394.13	A_g	2394.36	A_1	2424.58	A_{1g}	2454.73
0^u	2^1	B_{1g}	21.89	A_1	22.97	B_2	24.03	A_g	24.12	A_1	25.18	B_{1g}	26.32
1^l	2^2	A_{1g}	209.15	A_1	212.07	A_1	215.12	A_g	215.02	A_1	218.21	A_{1g}	221.46
1^u	2^3	B_{1g}	353.36	A_1	359.70	B_2	366.30	A_g	366.04	A_1	372.91	B_{1g}	379.81
2^l	4^2+2^4	A_{1g}	534.62	A_1	541.69	A_1	548.57	A_g	548.48	A_1	555.21	A_{1g}	561.76
2^l	2^4+4^2	A_{1g}	556.36	A_1	565.28	A_1	574.68	A_g	574.33	A_1	584.23	A_{1g}	594.27
2^u	2^14^2	B_{1g}	566.79	A_1	574.14	B_2	581.37	A_g	581.52	A_1	588.60	B_{1g}	595.82
3^l	2^24^2	A_{1g}	724.64	A_1	733.43	A_1	742.22	A_g	742.18	A_1	750.99	A_{1g}	759.88
2^u	2^5	B_{1g}	765.29	A_1	778.55	B_2	792.32	A_g	791.72	A_1	806.02	B_{1g}	820.25
3^u	2^34^2	B_{1g}	860.94	A_1	872.57	B_2	884.35	A_g	884.17	A_1	896.09	B_{1g}	908.12
4^l	$2^6+2^44^2$	A_{1g}	988.01	A_1	1002.77	A_1	1017.65	A_g	1017.13	A_1	1032.12	A_{1g}	1046.72
5^l	$5^1+2^15^1$	E_u	1030.05	A_1	1041.37	A_1	1053.05	B_{2u}	1054.31	A_1	1066.36	E_u	1080.72
5^l	$5^1+2^15^1$	E_u	1030.11	B_2	1042.35	B_2	1054.11	B_{3u}	1057.15	B_2	1068.28	E_u	1080.81
4^l	$2^44^2+2^6+4^4$	A_{1g}	1036.31	A_1	1052.02	A_1	1068.21	A_g	1067.52	A_1	1084.36	A_{1g}	1101.17
4^l	$4^4+2^44^2$	A_{1g}	1094.36	A_1	1107.79	A_1	1121.15	A_g	1120.98	A_1	1134.45	A_{1g}	1147.90
4^u	2^14^4	B_{1g}	1102.23	A_1	1115.63	B_2	1128.67	A_g	1128.85	A_1	1141.72	B_{1g}	1154.72
6^l	1^1	A_{1g}	1135.76	A_1	1148.43	A_1	1161.16	A_g	1163.19	A_1	1175.44	A_{1g}	1190.15
6^u	2^11^1	B_{1g}	1159.79	A_1	1172.51	B_2	1184.79	A_g	1189.93	A_1	1202.63	B_{1g}	1218.94
5^u	$5^1+2^15^1$	E_u	1196.03	A_1	1199.80	A_1	1213.39	B_{3u}	1223.80	B_2	1227.26	E_u	1252.36
5^u	$2^15^1+5^1$	E_u	1196.08	B_2	1214.26	B_2	1222.48	B_{2u}	1225.18	A_1	1242.74	E_u	1252.41
7^l	3^1	B_{2g}	1198.45	B_2	1218.12	A_1	1242.11	B_{1g}	1225.75	B_2	1249.36	B_{2g}	1255.58
4^u	$2^54^2+2^7+2^14^4$	B_{1g}	1206.48	A_1	1223.05	B_2	1239.72	A_g	1239.24	A_1	1256.19	B_{1g}	1272.89
7^u	2^13^1	A_{2g}	1217.94	B_2	1239.47	B_2	1255.99	B_{1g}	1250.60	B_2	1267.22	A_{2g}	1279.17
8^l	2^24^4	A_{1g}	1239.17	A_1	1253.93	A_1	1268.42	A_g	1268.36	A_1	1282.89	A_{1g}	1297.43
4^u	$2^7+2^54^2$	B_{1g}	1282.67	A_1	1303.99	B_2	1326.08	A_g	1325.64	A_1	1347.35	B_{1g}	1372.28
9^l	2^25^1	E_u	1302.35	B_2	1316.58	A_1	1327.45	B_{2u}	1333.96	A_1	1349.56	E_u	1367.28
9^l	2^25^1	E_u	1302.60	A_1	1317.14	B_2	1336.11	B_{3u}	1336.05	B_2	1350.94	E_u	1367.62
10^l	2^21^1	A_{1g}	1344.13	A_1	1363.58	A_1	1382.20	A_g	1377.86	A_1	1397.03	A_{1g}	1411.39
8^u	$2^34^4+2^54^2$	B_{1g}	1378.39	A_1	1396.31	B_2	1414.12	A_g	1413.88	A_1	1431.98	B_{1g}	1450.08
11^l	2^54^2	A_{1g}	1405.12	A_1	1423.42	A_1	1441.83	A_g	1441.19	A_1	1459.89	A_{1g}	1478.86
12^l	2^23^1	B_{2g}	1408.77	B_2	1426.58	A_1	1444.26	B_{1g}	1443.22	B_2	1460.98	B_{2g}	1477.24
9^u	2^35^1	E_u	1464.38	B_2	1480.50	B_2	1493.83	B_{2u}	1502.51	A_1	1518.89	E_u	1541.77
9^u	2^35^1	E_u	1464.59	A_1	1482.65	A_1	1505.27	B_{3u}	1503.46	B_2	1521.99	E_u	1542.01
10^u	2^31^1	B_{1g}	1492.89	A_1	1516.85	B_2	1539.38	A_g	1533.56	A_1	1557.49	B_{1g}	1574.50
13^l	$2^3+2^44^4$	A_{1g}	1529.39	A_1	1551.44	A_1	1573.32	A_g	1572.68	A_1	1594.87	A_{1g}	1616.48
12^u	2^33^1	A_{2g}	1548.39	B_2	1570.28	B_2	1591.98	B_{1g}	1589.64	B_2	1611.41	A_{2g}	1631.25
13^l	$2^3+2^64^2+2^44^4$	A_{1g}	1567.62	A_1	1592.47	A_1	1619.08	A_g	1618.13	A_1	1645.58	A_{1g}	1673.27
14^l	$4^25^1+2^14^25^1$	E_u	1574.33	A_1	1591.47	A_1	1609.47	B_{2u}	1610.52	A_1	1629.39	E_u	1649.15
14^l	$4^25^1+2^14^25^1$	E_u	1574.85	B_2	1594.93	B_2	1611.28	B_{3u}	1614.34	B_2	1631.45	E_u	1649.69

[a]The first column lists pairs of levels split by the B_{1g} (D_{4h}) motion. The l and u labels designate lower and upper levels, respectively. The vibrational quantum numbers of the b_{1g} distortion mode in the u and l vibrational configurations differ by one. The pairs are numbered according to increasing wave numbers. When two levels correspond to the same combination of vibrational configurations, they are attributed to the same pair. Second column gives the leading harmonic vibrational configurations of the wave function.

B_{2u} fundamentals will also be populated, the cycle will undergo a complex motion including the out-of-plane bending.

The term pattern is complicated by the presence of strong anharmonic resonances. In the A' block, for instance, the harmonic states with two quanta in the B_{1g} distortion and two quanta in the out-of-plane B_{2u} form a lower (2^l in Table III) anharmonic pair at 535 and 556 cm^{-1} in $^{11}B_4$, their upper counterparts (2^u) are calculated to lie at 567 and 765 cm^{-1}. In the A'' block the 3^l pair lies at 780 and 823 cm^{-1}, the 3^u pair at 836 and 992 cm^{-1}. The assignments of the split states becomes difficult going up the ladder and the attribution to the upper and lower levels in Tables III and IV are only tentative. Similar resonances exist also in other isotopomers. The calculations yield essentially identical vibrational energies for the two possible C_{2v} rhombic isotopomers $^{10}B_2{}^{11}B_2$, but the anharmonic couplings lead to shifts particularly in the region of the E modes.

IV. SUMMARY AND CONCLUSION

To date, only the photodetachment spectrum of rhombic B_4^- has yielded experimental information on the ground state of B_4. The detected band is broad with no distinguishable vibrational progression.[30]

In the present work we used a double minimum six-dimensional CCSD(T) PES for the lowest isomer of B_4 to solve the anharmonic nuclear motion problem by the MULTIMODE approach. The calculated splittings of the fundamental levels (around 20 cm^{-1}) indicate that the rhombic structure rearranges on the time scale of about 0.75 ps. The presence of the splittings, anharmonic resonances, hot bands, and

TABLE IV. Vibrational pattern in the B_4 isotopomers (A'' symmetry).

Abundance (%)		$^{11}B_4$ 41.2		$^{10}B^{11}B_3$ 40.9		$^{10}B_2{}^{11}B_2$ 10.2		$^{10}B_2{}^{11}B_2$ 5.1		$^{10}B_3{}^{11}B$ 2.5		$^{10}B_4$ 0.2	
Assignment[a]		D_{4h}		C_{2v}		C_{2v}		D_{2h}		C_{2v}		D_{4h}	
1^l	4^1	B_{2u}	271.28	B_1	274.43	A_2	277.53	B_{1u}	277.53	B_1	280.58	B_{2u}	283.62
1^u	2^14^1	A_{2u}	295.18	B_1	299.42	B_1	303.61	B_{1u}	303.72	B_1	307.84	A_{2u}	312.05
2^l	2^24^1	B_{2u}	467.28	B_1	473.17	A_2	479.13	B_{1u}	479.06	B_1	485.11	B_{2u}	491.22
2^u	2^34^1	A_{2u}	607.22	B_1	616.13	B_1	625.21	B_{1u}	625.02	B_1	634.27	A_{2u}	643.60
3^l	$2^44^1+4^3$	B_{2u}	780.37	B_1	791.07	A_2	801.78	B_{1u}	801.55	B_1	812.29	B_{2u}	822.90
3^l	$4^3+2^44^1$	B_{2u}	822.86	B_1	833.33	A_2	843.89	B_{1u}	843.76	B_1	854.47	B_{2u}	865.25
3^u	2^14^3	A_{2u}	835.88	B_1	846.24	B_1	856.40	B_{1u}	856.56	B_1	866.54	A_{2u}	876.64
4^l	2^24^3	B_{2u}	981.52	B_1	993.24	A_2	1004.87	B_{1u}	1004.77	B_1	1016.40	B_{2u}	1028.04
3^u	2^54^1	A_{2u}	992.46	B_1	1006.94	B_1	1021.72	B_{1u}	1021.29	B_1	1036.35	A_{2u}	1051.39
4^u	$2^34^3+2^54^1$	A_{2u}	1115.54	B_1	1130.13	B_1	1144.74	B_{1u}	1144.47	B_1	1159.28	A_{2u}	1174.07
5^l	$2^64^1+2^44^3$	B_{2u}	1197.32	B_1	1213.67	A_2	1230.10	B_{1u}	1229.56	B_1	1246.27	B_{2u}	1262.71
5^l	$2^44^3+2^64^1+4^5$	B_{2u}	1289.36	B_1	1307.33	A_2	1325.39	B_{1u}	1325.11	B_1	1343.75	B_{2u}	1362.26
6^l	$4^15^1+2^14^15^1$	E_g	1304.69	B_1	1318.96	B_1	1334.22	B_{2g}	1335.00	B_1	1351.02	E_g	1367.67
6^l	$4^15^1+2^14^15^1$	E_g	1304.92	A_2	1321.52	A_2	1335.22	B_{3g}	1338.43	A_2	1352.50	E_g	1368.00
5^u	$2^14^5+2^54^3$	A_{2u}	1361.90	B_1	1379.49	B_1	1395.76	B_{1u}	1394.47	B_1	1411.52	A_{2u}	1426.89
7^l	$4^5+2^44^3$	B_{2u}	1367.46	B_1	1384.22	A_2	1400.32	B_{1u}	1400.21	B_1	1416.46	B_{2u}	1432.42
8^l	4^11^1	B_{2u}	1404.14	B_1	1419.99	A_2	1436.04	B_{1u}	1437.81	B_1	1453.30	B_{2u}	1470.65
7^u	$2^74^1+2^14^5+2^54^3$	A_{2u}	1422.01	B_1	1441.26	B_1	1459.93	B_{1u}	1459.21	B_1	1478.49	A_{2u}	1496.97
8^u	$2^14^11^1$	A_{2u}	1430.78	B_1	1445.73	B_1	1461.06	B_{1u}	1467.04	B_1	1481.89	A_{2u}	1502.25
9^l	4^13^1	A_{1u}	1457.21	A_2	1467.30	A_2	1483.37	A_u	1490.28	A_2	1502.05	A_{1u}	1525.70
6^u	$4^15^1+2^14^15^1$	E_g	1467.38	B_1	1484.31	B_1	1497.54	B_{2g}	1501.83	B_1	1521.77	E_g	1535.96
6^u	$4^15^1+2^14^15^1$	E_g	1467.87	A_2	1489.35	A_2	1514.14	B_{3g}	1502.88	A_2	1524.04	E_g	1536.47
9^u	$2^14^13^1$	B_{1u}	1479.48	A_2	1506.38	B_1	1525.63	A_u	1517.84	A_2	1538.05	B_{1u}	1552.26
10^l	2^24^5	B_{2u}	1506.03	B_1	1525.82	A_2	1543.72	B_{1u}	1542.09	B_1	1561.12	B_{2u}	1577.91
5^u	$2^74^1+2^54^3$	A_{2u}	1521.18	B_1	1543.74	B_1	1566.79	B_{1u}	1565.99	B_1	1589.85	A_{2u}	1613.24
11^l	$2^24^15^1$	E_g	1562.59	B_1	1580.29	B_1	1593.11	B_{2g}	1600.07	B_1	1618.21	E_g	1639.02
11^l	$2^24^15^1$	E_g	1563.18	A_2	1581.59	A_2	1602.56	B_{3g}	1602.41	A_2	1620.06	E_g	1639.61

[a]See footnote in Table III.

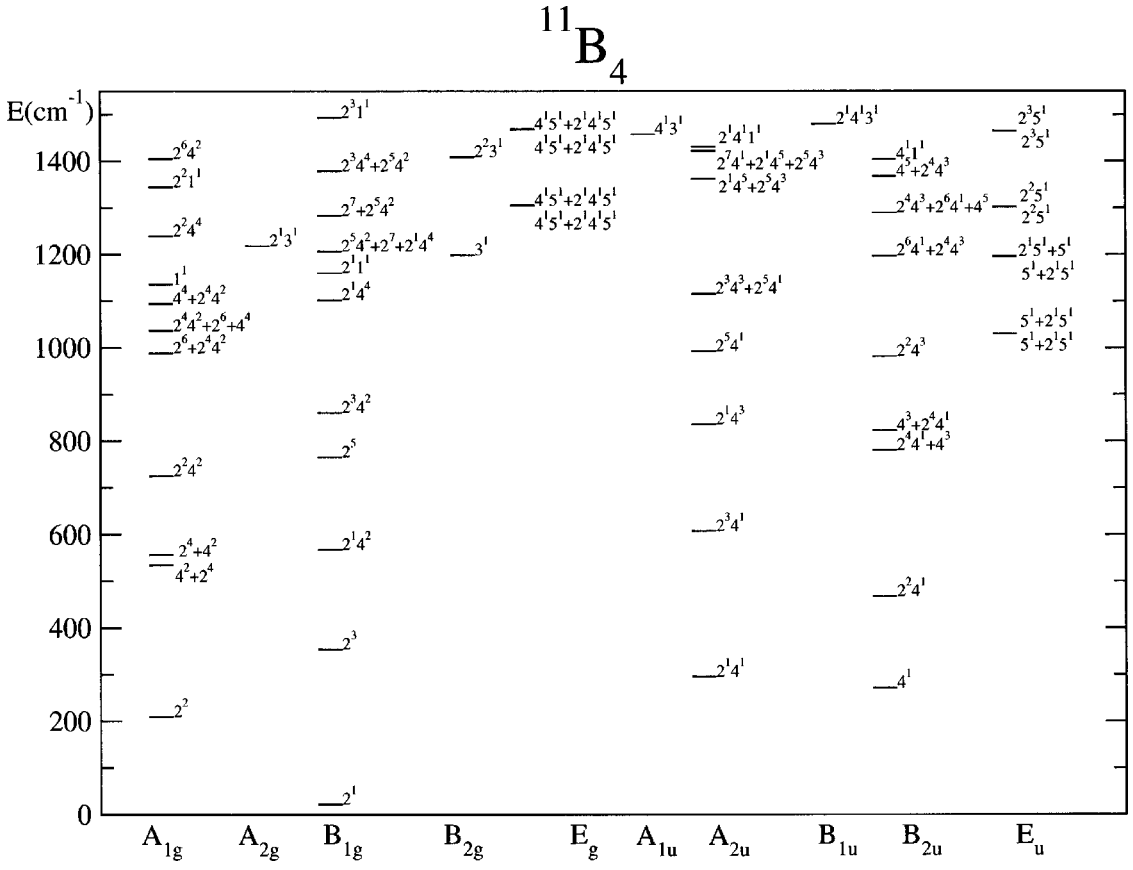

FIG. 3. Vibrational energy pattern in $^{11}B_4$ up to 1500 cm^{-1}. The vibrational states are assigned using irreducible representations of the D_{4h} point group.

complex rotational structures with different nuclear spin statistics will considerably complicate the assignments of the gas phase IR and Raman spectra at 298 K. Some of the dipole forbidden transitions are allowed in the less abundant isotopomers and will have their own weak rotational transitions. The theoretical approach developed in this work is generally applicable for tetraatomic rhombic clusters not exhibiting the Jahn–Teller effect.

ACKNOWLEDGMENTS

This work was supported by the Office of Aerospace Research and Development and the Swiss National Science Foundation (Project 200020-100019). S.C. would like to acknowledge the support of the U.S. Office of Naval Research through Grant N00014-01-1-0809. The authors thank R. Marquardt for stimulating discussions.

[1] R. N. Grimes, J. Chem. Educ. **81**, 658 (2004).
[2] J. Berkowitz and W. A. Chupka, J. Chem. Phys. **40**, 2735 (1964).
[3] L. Hanley, J. L. Whitten, and S. L. Anderson, J. Phys. Chem. **92**, 5803 (1988).
[4] S. A. Ruatta, L. Hanley, and S. L. Anderson, J. Chem. Phys. **91**, 226 (1989).
[5] P. A. Hintz, S. A. Ruatta, and S. L. Anderson, J. Chem. Phys. **92**, 292 (1990).
[6] S. J. La Placa, P. A. Roland, and J. J. Wynne, Chem. Phys. Lett. **190**, 163 (1992).
[7] M. B. Sowa-Resat, J. Smolanoff, A. Lapicki, and S. L. Anderson, J. Chem. Phys. **106**, 9511 (1977).
[8] K. P. Huber and G. Herzberg, *Constants of Diatomic Molecules* (Van Nostrand Reinhold, New York, 1979).
[9] S. Tam, M. Macler, M. E. DeRose, and M. E. Fajardo, J. Chem. Phys. **113**, 9067 (2000).
[10] R. Krishnan and J. A. Pople, Int. J. Quantum Chem. **14**, 91 (1978).
[11] H. W. Jin and Q. S. Li, Phys. Chem. Chem. Phys. **5**, 1110 (2003).
[12] Q. S. Li and H. W. Jin, J. Chin. Chem. Soc. (Taipei) **50**, 1115 (2003).
[13] G. H. Jeong, R. Boucher, and K. J. Klabunde, J. Am. Chem. Soc. **112**, 3332 (1990).
[14] P. A. Hintz, M. B. Sowa, S. A. Ruatta, and S. L. Anderson, J. Chem. Phys. **94**, 6446 (1991).
[15] A. C. Tang, Q. S. Li, C. W. Liu, and J. Li, Chem. Phys. Lett. **201**, 465 (1993).
[16] A. Ricca and C. W. Bauchschlicher, Chem. Phys. **208**, 233 (1966).
[17] Z. X. Wang and M. B. Huang, J. Am. Chem. Soc. **120**, 6758 (1988).
[18] J. E. Fowler and J. M. Ugalde, J. Phys. Chem. A **104**, 397 (2000).
[19] E. D. Jemmis and M. M. Balakrishnarajan, J. Am. Chem. Soc. **123**, 4324 (2001).
[20] A. N. Alexandrova, A. I. Boldyrev, H.-J. Zhai, L.-S. Wang, E. Heiner, and P. W. Fowler, J. Phys. Chem. A **107**, 1359 (2003), and references therein.
[21] Q. S. Li, L. F. Gong, and Z. M. Gao, Chem. Phys. Lett. **390**, 220 (2004).
[22] I. Boustani, Phys. Rev. B **55**, 16426 (1997).
[23] I. Boustani, Chem. Phys. Lett. **233**, 273 (1995).
[24] H. Reis and M. G. Papadopoulos, J. Comput. Chem. **20**, 679 (1999).
[25] J. M. L. Martin, J. P. Francois, and R. Gijbels, Chem. Phys. Lett. **189**, 529 (1992).
[26] H. Kato and E. Tanaka, J. Comput. Chem. **12**, 1097 (1991).
[27] H. Kato and E. Tanaka, J. Chem. Soc. Jpn. **8**, 1183 (1989).
[28] A. K. Ray, I. A. Howard, and K. M. Kanal, Phys. Rev. B **45**, 14247 (1992).
[29] M. Wyss, E. Riaplov, A. Batalov, J. P. Maier, T. Weber, W. Meyer, and P. Rosmus, J. Chem. Phys. **119**, 9703 (2003).
[30] H.-J. Zhai, L.-S. Wang, A. N. Alexandrovna, A. I. Boldyrev, and V. G. Zakrzewski, J. Phys. Chem. A **107**, 9319 (2003), and references therein.
[31] H. A. Jahn and E. Teller, Proc. R. Soc. London **A161**, 220 (1937); H. Sponer and E. Teller, Rev. Mod. Phys. **13**, 75 (1941).
[32] G. Herzberg, *Molecular Spectra and Molecular Structure* (Van Nostrand Reinhold, New York, 1966), Vol. III.
[33] R. G. Pearson, J. Am. Chem. Soc. **91**, 4947 (1969).
[34] J. M. L. Martin, T. Lee, and P. Taylor, J. Chem. Phys. **97**, 8361 (1992).
[35] H. Lin, W. Thiel, S. Yurchenko, M. Carvajal, and P. Jensen, J. Chem. Phys. **117**, 11265 (2002).
[36] T. Rajamäki, A. Miani, and L. Halonen, J. Chem. Phys. **118**, 10929 (2003).
[37] J. Boustani, W. Pewestorf, P. Fantuci, V. Bonacic-Koutecky, and J. Koutecky, Phys. Rev. B **35**, 9437 (1987).
[38] R. Rousseau and D. Marx, Phys. Rev. A **56**, 617 (1997).
[39] J. D. Watts, J. Gauss, J. F. Stanton, and R. J. Bartlett, J. Chem. Phys. **97**, 8372 (1992), and references therein.
[40] K. Balasubramanian, P. Y. Feng, and M. Z. Liao, J. Chem. Phys. **91**, 3561 (1989).
[41] S. F. Chekmarev, R. Mitric, and V. Bonacic-Koutecky, Eur. Phys. J. D **24**, 45 (2003).
[42] M. C. McCarthy, A. J. Apponi, and P. Thaddeus, J. Chem. Phys. **110**, 10645 (1999); A. J. Apponi, M. C. McCarthy, C. A. Gottlieb, and P. Thaddeus, *ibid.* **111**, 3911 (1999); M. C. McCarthy, A. J. Apponi, and P. Thaddeus, *ibid.* **111**, 7175 (1999).
[43] S. Carter, S. Culik, and J. M. Bowman, J. Chem. Phys. **107**, 10458 (1997).
[44] C. Léonard, N. C. Handy, S. Carter, and J. M. Bowman, Spectrochim. Acta, Part A **58**, 825 (2002).
[45] N. C. Handy, S. Carter, and S. M. Colwell, Mol. Phys. **96**, 477 (1999).
[46] S. Carter and N. C. Handy, J. Chem. Phys. **113**, 987 (2000).
[47] MOLPRO is a package of *ab initio* programs written by H.-J. Werner and P. J. Knowles, further information from http://www.molpro.net/
[48] P. J. Knowles, C. Hampel, and H.-J. Werner, J. Chem. Phys. **99**, 5219(E) (1993); **112**, 3106 (2000).
[49] T. H. Dunning, J. Chem. Phys. **90**, 1007 (1989); R. A. Kendall, T. H. Dunning, and R. J. Harrison, *ibid.* **96**, 6796 (1992).
[50] J. F. Stanton and R. J. Bartlett, J. Chem. Phys. **98**, 7029 (1993).
[51] H.-J. Werner and P. J. Knowles, J. Chem. Phys. **82**, 5053 (1985); Chem. Phys. **115**, 259 (1985).
[52] See EPAPS Document No. E-JCPSA6-122-010501 for getting the analytic form of the potential. A direct link to this document may be found in the online article's HTML reference section. The document may also be reached via the EPAPS homepage (http://www.aip.org/pubservs/epaps.html) or from ftp.aip.org in the directory /epaps/. See the EPAPS homepage for more information.
[53] S. Carter, J. M. Bowman, and N. C. Handy, Theor. Chem. Acc. **100**, 191 (1998).
[54] J. K. G. Watson, Mol. Phys. **15**, 479 (1968).
[55] D. O. Harris, G. O. Engerholm, and W. Gwinn, J. Chem. Phys. **43**, 1515 (1965).

Z. Phys. Chem. **219** (2005) 467–480

Theoretical Study of the Electronically Excited States of B_4, B_4^+ and B_4^-

By Claire Gillery[1], Roberto Linguerri[1], Pavel Rosmus[1,*], and John P. Maier[2]

[1] Laboratoire de Chimie Théorique, Université de Marne la Vallée, F-77454 Champs sur Marne, France
[2] Department of Chemistry, University of Basel, Klingelbergstr. 80, CH-4056 Basel, Switzerland

(Received January 18, 2005; accepted January 25, 2005)

Electronical Exitation Energies / Conical Intersections / Cluster UV Spectra / Electron Affinity / Ionization Energy

First-principle full valence complete active space calculations (CASSCF) are reported for the electronic states of the D_{2h} and C_{2v} planar isomers of B_4, B_4^+ and B_4^-. This approach is found to reproduce well the experimentally known transition energies for the two lowest excited triplet states of the most stable rhombic B_4 isomer. The pattern of electronic transitions up to about 4.5 eV for B_4 singlet and B_4^+ doublet states calculated in similar way should guide an UV spectroscopic search.

1. Introduction

Studies of small boron clusters are motivated by a desire to understand the manifold of chemical structures, intramolecular dynamics and reactivity of these covalently bound homonuclear molecules. There are surprisingly few reports on the spectroscopy of such neutral or charged clusters. The boron trimer was investigated in low temperature matrices by ESR [1], IR [2] and UV [3] techniques. So far only its $2\ ^2E' \leftarrow X\ ^2A_1'$ electronic transition was observed in the gas phase [4]. The B_3 and B_4 clusters in their neutral and anionic forms were studied by photoelectron spectroscopy [5]. The first ionization energy [6–8] and the electron affinity [5] of rhombic B_4 are known. The mass-spectrometric studies [9–11] on B_n^+ provided information about their thermochemical stabilities and fragmentation paths.

The present contribution deals mainly with electronically excited states of B_4 and B_4^+. The aim is to calculate the pattern of electronic transitions in

* Corresponding author. E-mail: rosmus@univ-mlv.fr

rhombic and planar C_{2v} isomers to guide the spectroscopic search for these molecules. Previous theoretical works have reported the ground state equilibrium structures of various isomers, their relative stabilities, harmonic frequencies, nuclear-independent chemical shifts, dipole polarizability, hyperpolarizability, and thermochemical data [12–31]. Recently we have investigated the splittings of vibrational states in rhombic B_4 [30]. So far the only theoretical study concerning the electronically excited triplet and singlet states of B_4 was performed in conjunction with the assignment of the B_4^- photoelectron spectrum [5].

The boron tetramer represents a challenging problem from the point of view of electronic spectroscopy. Depending on its formation different isomers could coexist and their electronic states could lie in the same UV region. The states in rhombic isomers can correlate with electronically degenerate states of D_{4h} symmetry forming Jahn–Teller pairs. Perturbations can arise from vibronic couplings and spin multiplet crossings. As in the B_4 rhombic ground state [30], the minimum/square transition state topology of the potential energy surface (PES) can lead to splittings of vibrational modes complicating the vibronic coupling effects.

The present study shows that the ground states of B_4^+ and B_4^- consist of two vibronically coupled electronic states. The most intense electronic transitions in B_4 and B_4^+ will be those to Jahn–Teller states. It is found that the pattern of dipole allowed electronic transitions in rhombic and C_{2v} isomers should allow them to be recognized by their UV spectra.

2. Computational approach

All electronic structure calculations were carried out using the MOLPRO program [32]. The valence electronic configurations for the lowest isomers of the B_4 electronic ground state are:

$$\mathrm{X}\ {}^1\mathrm{A}_g\ (\mathrm{D}_{2h}\ \text{rhombus})\ 1\mathrm{a}_g^2\,1\mathrm{b}_{2u}^2\,1\mathrm{b}_{3u}^2\,1\mathrm{b}_{1u}^2\,1\mathrm{b}_{1g}^2\,2\mathrm{a}_g^2$$

$$\mathrm{X}\ {}^1\mathrm{A}_1\ (\mathrm{C}_{2v}\ \text{planar})\ 1\mathrm{a}_1^2\,2\mathrm{a}_1^2\,1\mathrm{b}_1^2\,3\mathrm{a}_1^2\,1\mathrm{b}_2^2\,4\mathrm{a}_1^2$$

$$\mathrm{X}\ {}^1\Sigma_g^+\ (D_{\infty h})\ 1\sigma_g^2\,1\sigma_u^2\,2\sigma_g^2\,1\pi_u^4\,2\sigma_u^2\,.$$

In the calculations of equilibrium geometries vertical and adiabatic excitation energies we used the CASSCF or state-averaged CASSCF methods [33]. In the present work the stationary points optimization was restricted to planar (D_{2h}, D_{4h}, C_{2v}) or linear centro-symmetric structures. It has been known in previous calculations [12] that rhombic, planar C_{2v} and centro-symmetric structures represent local minima on the ground state PES of B_4, B_4^+ and B_4^-. For the B_4^+ linear structure the symmetry of the ground state has been calculated to be ${}^2\Sigma_g$ [12] and ${}^2\Sigma_u$ [31], whereas the present CASSCF calculations yield a ${}^2\Pi_u$ state. In the case of the B_4^- ground state a ${}^2\Pi_g$ state has been

obtained [12]; we find on the other hand the lowest centro-symmetric linear isomer to have the $^2\Pi_u$ symmetry. The EOM-CC method [34] was also employed for the B_4 excited singlet states and some of the energy differences were calculated by the RCCSD(T) approach [35]. In most calculations the basis set used was the augmented correlation-consistent polarized valence triple zeta (aug-cc-pVTZ) [36]. The relative energies of the isomers, the ionization energy and the electron affinity were calculated by the RCCSD(T) method and the aug-cc-pVQZ basis set [36]. Our most reliable excitation energies were obtained by the full valence CASSCF method for each state of a given irreducible representation calculated separately. For singlet states the full valence active space comprised about 1.7×10^6 CSF's for the rhombic and 3.5×10^6 CSF's for the planar C_{2v} structures. More information about the computations is specified in the footnotes of Tables 1 to 7.

3. Results and discussion

The optimized D_{2h} and C_{2v} planar or centro-symmetric linear stationary points on the six-dimensional PES of the electronic ground and excited states for B_4, B_4^+ and B_4^- are given in Tables 1 to 3. The geometry parameters and symmetry axes are defined in Fig. 1. The calculated vertical and adiabatic electronic excitation energies are compiled in Tables 4 to 7. The RCCSD(T) relative energy differences between the optimized structures for the three isomers show that in all three species the most stable isomers have rhombic structures followed by planar C_{2v} structures which lie 2.18 eV (B_4), 1.09 eV (B_4^+), 1.55 eV (B_4^-) (Tables 1 to 3) higher in energy, in relatively good agreement with previous theoretical findings (*cf*. Ref. [12]). The lowest dissociation energy ($B^+(^1S) + B_3$ ($X\ ^2A_1'$)) has been determined experimentally to be 2.4 ± 0.6 eV [6], though the theoretical value was calculated several eV larger [17, 29]. The ground state PES at optimized geometries of the three isomers of B_4^+ lies below this asymptotic limit. The rhombus/square energy difference of 0.031 eV on the double minimum potential of the electronic ground state of B_4 leads to splittings of vibrational transitions [30]. In B_4^+ (^2A_g) the barrier to the square transition state is calculated to be ten times smaller and will not lead to such splittings (Table 2 and [17]). In the ^2A_g state of B_4^- this barrier is almost three times larger (0.082 eV, Table 3) and thus the splittings will be smaller than in rhombic B_4. In the geometry region of the square saddle point of the B_{3u} state the negative ion is calculated to be unstable with respect to autoionization. The B_{2u} state correlating with the corresponding E_u state autoionizes already in the geometry region of the B_{3u} minimum.

In B_4^+ the lowest ^2A_g state lies only 0.17 eV below the $^2B_{1g}$ state (Table 6, method e). Both states cross in D_{2h} structures along the ring angle coordinate (Fig. 2a), and form an avoided crossing along the b_{1g} coupling mode one (Fig. 2b). The accuracy of the *ab initio* calculated energy differences and

Table 1. CASSCF optimized geometries for the B_4 isomers and relative energy differences between their minima.

	B_4 (D_{2h}) rhombus				B_4 (D_{4h}) square		
State	Method	R [bohr]	α [deg.]	$\Delta E_{CCSD(T)}$ [a] [eV]	Method	R [bohr]	$\Delta E_{CCSD(T)}$ [a] [eV]
X ^1A_g	*b*	2.909	75.8	0	*b*	2.899	0.031
$^1B_{1u}$	*c*	3.134	73.9		*c*	3.266	
$^1B_{1g}$	*c*	3.092	61.7		*c*	3.033	
$^1B_{3u}$	*c*	3.007	69.8		*c*	3.007	
$^1B_{3g}$	*c*	3.058	60.3		*c*	2.981	
$^1B_{2g}$	*c*	3.060	64.7		*c*	2.981	
$^1B_{2u}$	*c*	3.024	59.4		*c*	3.007	
^1A_u	*c*	3.300	90.0		*c*	3.300	

	B_4 (C_{2v})				
State	Method	R_1 [bohr]	R_2 [bohr]	θ [deg.]	$\Delta E_{CCSD(T)}$ [a] [eV]
X $^1A_1$	*d*	3.227	3.026	56.8	2.182
	e	3.253	2.986	58.4	
$^1B_2$	*f*	3.386	3.218	54.4	
$^1B_1$	*f*	2.936	3.100	58.3	
$^1A_2$	*f*	3.207	3.205	55.2	
$^1A_1$	*f*	3.111	3.174	54.6	

	B_4 ($D_{\infty h}$) linear			
State	Method	R_1 [bohr]	R_2 [bohr]	$\Delta E_{CCSD(T)}$ [a] [eV]
X $^1\Sigma_g^+$	*g*	2.922	2.890	2.379

[a] $\Delta E_{CCSD(T)}$ relative to the X ^1A_g state of rhombic B_4; aug-cc-VQZ basis set; $E = -98.91001460$ hartree.
b CCSD(T) with aug-cc-VQZ basis set.
c CASSCF with aug-cc-VTZ basis set; active space: 1-3a_g, 1-2b_{3u}, 1-2b_{2u}, 1-2b_{1u}, 1-2b_{1g}, 1b_{2g}, 1b_{3g}.
d CASSCF with aug-cc-VTZ basis set; active space: 1-6a_1, 1-3b_1, 1-3b_2.
e CCSD(T) with aug-cc-VTZ basis set.
f CASSCF with aug-cc-VTZ basis set; active space: 1-7a_1, 1-3b_1, 1-3b_2, 1a_2.
g CASSCF with aug-cc-VTZ basis set; active space: 1-3a_g, 1-3b_{3u}, 1-2b_{2u}, 1-2b_{1u}, 1b_{1g}, 1b_{2g}.

geometries does not permit a definite answer about the mixing of both states, *i.e.* about the structure of the vibronic ground state, vibronic transitions and intensity borrowing in the UV absorption spectra.

Table 2. CASSCF optimized geometries for the B_4^+ isomers and relative energy differences between their minima.

	B_4^+ (D_{2h}) rhombus				B_4^+ (D_{4h}) square		
State	Method	R [bohr]	α [deg.]	$\Delta E_{\mathrm{RCCSD(T)}}$ [a] [eV]	Method	R [bohr]	$\Delta E_{\mathrm{RCCSD(T)}}$ [a] [eV]
X ^2A_g	*b*	2.958	79.5	0	*b*	2.913	0.003
	c	2.951	83.4				
$^2B_{1u}$	*d*	3.026	76.1		*d*	3.003	
$^2B_{1g}$	*d*	3.036	61.6		*d*	2.954	
$^2B_{3u}$	*d*	3.127	54.2		*d*	3.030	
$^2B_{2u}$	*d*	N.C.	N.C.		*d*	3.030	
$^2B_{3g}$	*d*	3.060	77.6		*d*	3.155	
$^2B_{2g}$	*d*	3.152	65.3		*d*	3.155	
^2A_u	*d*	3.247	64.4		*d*	3.159	

	B_4^+ (C_{2v})				
State	Method	R_1 [bohr]	R_2 [bohr]	θ [deg.]	$\Delta E_{\mathrm{RCCSD(T)}}$ [a] [eV]
X $^2A_1$	*e*	3.113	3.087	56.5	1.087
	c	3.086	3.039	57.3	
$^2B_2$	*f*	3.602	3.149	57.1	
$^2B_1$	*f*	2.978	2.986	121.2	
$^2A_1$	*f*	3.081	3.017	61.5	
$^2B_1$	*f*	3.157	3.169	54.1	
$^2B_2$	*f*	3.187	3.196	56.7	

	B_4^+ ($D_{\infty h}$) linear			
State	Method	R_1 [bohr]	R_2 [bohr]	$\Delta E_{\mathrm{RCCSD(T)}}$ [a] [eV]
X $^2\Pi_u$	*g*	2.895	2.998	1.496

[a] $\Delta E_{\mathrm{RCCSD(T)}}$ relative to the X ^2A_g state of rhombic B_4^+; aug-cc-VQZ basis set; $E = -98.54990461$ hartree.

b CASSCF with aug-cc-VTZ basis set; active space: 1-3a_g, 1-2b_{3u},1-2b_{2u}, 1-2b_{1g}, 1-2b_{1u}.

c RCCSD(T) with aug-cc-VTZ basis set.

d CASSCF with aug-cc-VTZ basis set; active space: 1-3a_g, 1-2b_{3u}, 1-2b_{2u}, 1-2b_{1u}, 1-2b_{1g}, 1b_{2g}, 1b_{3g}; the optimization for the $^2B_{2u}$ state did not converge.

e CASSCF with aug-cc-VTZ basis set; active space: 1-7a_1, 1-2b_1, 1-3b_2.

f CASSCF with aug-cc-VTZ basis set; active space: 1-7a_1, 1-3b_1, 1-3b_2, 1a_2.

g CASSCF with aug-cc-VTZ basis set; active space: 1-3a_g, 1-3b_{3u}, 1-2b_{2u}, 1-2b_{1u}, 1b_{1g}, 1b_{2g}.

Table 3. CASSCF optimized geometries for the B_4^- isomers and relative energy differences between their minima.

State	B_4^- (D_{2h}) rhombus				B_4^- (D_{4h}) square		
	Method	R [bohr]	α [deg.]	$\Delta E_{RCCSD(T)}$ [a] [eV]	Method	R [bohr]	$\Delta E_{RCCSD(T)}$ [a] [eV]
X $^2B_{3u}$	*b*	2.992	63.3	0	*b*	2.922	
^2A_g	*c*	3.035	68.6	0.050	*c*	3.007	0.082

State	B_4^- (C_{2v})				
	Method	R_1 [bohr]	R_2 [bohr]	θ [deg.]	$\Delta E_{RCCSD(T)}$ [a] [eV]
X $^2A_1$	*d*	3.226	3.050	56.8	1.546
$^2B_1$	*e*	3.097	3.069	60.9	2.014

State	B_4^- ($D_{\infty h}$) linear			
	Method	R_1 [bohr]	R_2 [bohr]	$\Delta E_{RCCSD(T)}$ [a] [eV]
X $^2\Pi_u$	*f*	2.919	3.103	2.866

[a] $\Delta E_{RCCSD(T)}$ relative to the X $^2B_{3u}$ state of rhombic B_4^-; aug-cc-VQZ basis set; $E = -98.96948401$ hartree.
b CASSCF with aug-cc-VTZ basis set; active space: 1-3a_g, 1-3b_{3u}, 1-2b_{2u}, 1-2b_{1g}, 1-2b_{1u}.
c CASSCF with aug-cc-VTZ basis set; active space: 1-4a_g, 1-2b_{3u}, 1-2b_{2u}, 1-2b_{1g}, 1-2b_{1u}.
d CASSCF with aug-cc-VTZ basis set; active space: 1-7a_1, 1-4b_1, 1b_2.
e CASSCF with aug-cc-VTZ basis set; active space: 1-6a_1, 1-4 b_1, 1-3b_2.
f CASSCF with aug-cc-VTZ basis set; active space: 1-4a_g, 1-3b_{3u}, 1-2b_{2u}, 1-2b_{1u}, 1b_{1g}, 1b_{2g}.

Similar coupling is found also for the ground state of B_4^-. In the adiabatic picture the $^2B_{3u}$ state is calculated only 0.05 eV below the ^2A_g state (Table 3, and Ref. [5]). Also in this case both states cross in D_{2h} structures along the ring angle coordinate (Fig. 3a), and form an avoided crossing along the b_{3u} coupling mode (Fig. 3b).

The adiabatic aug-cc-pVQZ/RCCSD(T) ionization energy IE_e of B_4 has been calculated to be 9.799 eV for the rhombic, 8.705 eV for the planar C_{2v} and 8.916 eV for the linear structures using the optimized geometries (Tables 1 to 2). The first is in excellent agreement with the experimental value of 9.8 eV [2–4]. Similar approach yields adiabatic electron affinities of 1.618 eV (negative ion in $^2B_{3u}$ state) and 1.568 eV (in ^2A_g state) for the rhombic isomer, 1.786 eV (in $^2B_1$ state) and 2.254 eV (in $^2A_1$) for the C_{2v} isomer, and 1.131 eV (in $^2\Pi_u$ state) for the linear B_4^- (*cf*. also Ref. [12]). The two higher isomers

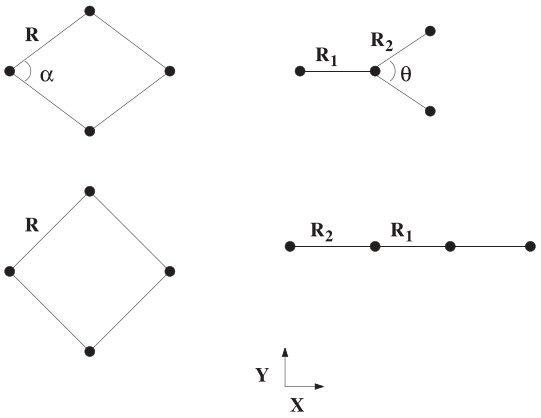

Fig. 1. Definition of the coordinates and symmetry axis in B_4 isomers.

have well defined electronic wavefunctions indicating that spontaneous electron detachment does not take place. The planar C_{2v} isomer ($^2A_1$) is calculated to lie just below the autodetachment threshold of 1.6 eV [5] (Table 3). The electronically excited states will autoionize, but the ground state six-dimensional PES has large portions on which the additional electron is bound, particularly along the isomerization paths.

The full valence CASSCF calculations of vertical excitation energies confirm that the ionization of B_4^- leads to triplet states of B_4 (Table 4). Our results agree well with the RCCSD(T) values [5], and with the positions of the first two observed bands in the photoelectron spectrum. This good agreement with experiment allows us to assume that other excitation energies calculated with this approach will be of similar accuracy.

The vibronic coupling in B_4^- ground state mixes gerade and ungerade wavefunctions. In its photoelectron spectrum only the ionizations to ungerade triplet states were assigned. In Table 4 we compare the vertical excitation energies relative to the singlet ground state of B_4 but calculated for the optimized geometries of the $^2B_{3u}$ and ^2A_g states of B_4^-. Whereas the energy differences for the first two triplet states agree nicely with experiment for the geometry of the $^2B_{3u}$ state, they disagree for the second structure. This supports the assumption made in [5] that the lowest part of the PES for the ground state of the negative ion is dominated by the $^2B_{3u}$ wavefunction. The lowest triplet states $^3B_{2u}$ and $^3B_{3u}$ correlate with the ^3E_u state in D_{4h} symmetry; the observed band corresponds to a Jahn–Teller system. The experimental spectrum at higher energies is more difficult to assign because several triplets and singlets are calculated to lie close to the observed band at about 2.4 eV (Table 4).

In Table 5 the vertical and adiabatic transition energies in rhombic and square geometries for the singlet states of B_4 are compared. Only one elec-

Table 4. Comparison of the experimental and calculated energy differences in B_4 at the optimized geometries of the $^2B_{3u}$ and ^2A_g states of rhombic B_4^-.

	T_v [a] [eV]	T_v [b] [eV]	T_v [c] [eV]	Experiment [eV]
X ^1A_g	0	0	0	0
a $^3B_{2u}$	1.29	2.18	1.29	1.09
b $^3B_{3u}$	1.43	1.95	1.39	1.42
c $^3B_{1g}$	1.64	1.84	1.74[d]	
A $^1B_{1g}$	2.03			
B $^1B_{2u}$	2.13			
d ^3A_g	2.55	1.75	1.60[d]	
e $^3B_{2g}$	2.60	2.80	2.50	
C $^1B_{2g}$	2.84			
f $^3B_{1u}$	2.85	2.37	2.18[d]	2.40
D $^1B_{1u}$	3.36			

[a] Full-valence CASSCF; aug-cc-pVTZ basis set; each state calculated separately at the optimized geometry of the X $^2B_{3u}$ state of B_4^-: $R = 3.015$ bohr, $\alpha = 63.6$ degrees [5]; $E = -98.69773452$ hartree.
[b] Full-valence CASSCF; aug-cc-pVTZ basis set; each state calculated separately at the optimized geometry of the X ^2A_g state of B_4^-: $R = 3.064$ bohr, $\alpha = 73.8$ degrees [5]; $E = -98.69847200$ hartree.
[c] RCCSD(T); each state calculated at the optimized geometry of the X $^2B_{3u}$ state of B_4^-: $R = 3.015$ bohr, $\alpha = 63.6$ degrees [5].
[d] RCCSD(T); each state calculated at the optimized geometry of the X ^2A_g state of B_4^-: $R = 3.064$ bohr, $\alpha = 73.8$ degrees [5].

Table 5. Vertical (T_v) and adiabatic (T_e) excitation energies and transition moments (μ_e) between singlet states of rhombic and square B_4.

	Rhombus					Square				
	$T_{v,av}$ [a] [eV]	μ_e [debye]	$T_{v,\mathrm{EOM}}$ [b] [eV]	T_v [c] [eV]	T_e [d] [eV]	$T_{v,av}$ [a] [eV]	μ_e [debye]	$T_{v,\mathrm{EOM}}$ [b] [eV]	T_v [c] [eV]	T_e [d] [eV]
X ^1A_g	0		0	0	0	0		0	0	0
A $^1B_{1g}$	2.91		3.12	2.94	2.12	2.98		3.35	3.10	2.87
B $^1B_{2u}$	3.44	0.6889 (y)	3.71	3.52	2.20	4.57	1.6642 (y)	4.63	4.56	4.19
C $^1B_{1u}$	3.56	0.2412 (z)	3.49	3.61	2.89	3.40	0.0000 (z)	3.43	3.46	3.30
D $^1B_{2g}$	3.74		3.74	3.77	2.94	5.19		4.48	5.30	4.68
E $^1B_{3u}$	3.99	2.3070 (x)	3.85	4.12	3.82	4.57	1.6642 (x)	4.63	4.56	4.19
F $^1B_{3g}$	4.66		4.55	4.58	3.90	5.19		4.48	5.30	4.68

[a] Full-valence SA-CASSCF with aug-cc-pVTZ basis set at the optimized geometry of X ^1A_g (Table 1); one state per irreducible representation calculated.
[b] At the optimized geometry of X ^1A_g (Table 1); aug-cc-pVQZ basis set.
[c] Full-valence CASSCF with aug-cc-pVTZ basis set at the optimized geometry of X ^1A_g (Table 1); each state calculated separately.
[d] Full-valence CASSCF with aug-cc-pVTZ basis set at optimized geometry (Table 1); each state calculated separately.

Table 6. Vertical (T_v) and adiabatic (T_e) excitation energies and transition moments (μ_e) between doublet and quartet states of rhombic and square B_4^+.

	Rhombus				Square			
	$T_{v,av}$ [a] [eV]	μ_e [b] [debye]	T_v [c] [eV]	T_e [d] [eV]	$T_{v,av}$ [a] [eV]	μ_e [b] [debye]	T_v [c] [eV]	T_e [d] [eV]
X ^2A_g	0		0					
A $^2B_{1g}$	0.58		0.70	0.17	0.73		0.78	0.74
B $^2B_{1u}$	0.63	0.9796 (z)	0.70	0.62	0.68	1.0374 (z)	0.75	0.60
a $^4B_{1g}$	1.99				2.13			
b $^4B_{1u}$	2.35				2.35			
C ^2A_g	2.50							
c $^4B_{2u}$	2.72	1.4404 (x)			3.94	1.1402 (x)		
D $^2B_{1u}$	2.93	0.2431 (z)						
E $^2B_{1g}$	2.94							
F $^2B_{3u}$	3.03	1.7305 (x)	3.04	1.64	3.69	0.7120 (x)	3.52	3.35
G $^2B_{2u}$	3.17	1.3820 (y)			3.69	0.7120 (y)	3.52	3.35
d $^4B_{2g}$	3.21				4.39			
e ^4A_u	3.28	0.8564 (z)			3.74	0.9007 (z)		
H $^2B_{2g}$	3.63		3.71	2.46	4.96		4.79	3.75
f $^4B_{3g}$	3.75				4.39			
I $^2B_{2u}$	3.81	0.6198 (y)						
J ^2A_u	4.07		4.15	2.93	4.68		4.44	3.48
g $^4B_{3u}$	4.13	0.1174 (y)			3.94	1.1402 (y)		
K ^2A_u	4.17							
L $^2B_{3u}$	4.28	0.8819 (x)						
M $^2B_{3g}$	4.31		4.44	3.86	4.96		4.79	3.75

[a] Full-valence SA-CASSCF with aug-cc-pVTZ basis set at the optimized geometry of X ^2A_g (Table 2); two states per irreducible representation calculated.
[b] For the quartet states the transition moments are given with respect to the lowest $^4B_{1g}$.
[c] Full-valence CASSCF with aug-cc-pVTZ at the optimized geometry of X ^2A_g (Table 2); each state calculated separately.
[d] Full-valence CASSCF with aug-cc-pVTZ basis set at optimized geometry (Table 2); each state calculated separately.

tronic state in a given irreducible representation has been considered. The state averaged calculations needed for the transition moments yield transition energies which deviate from those calculated for each state separately by less than about 0.1 eV. The CC-EOM vertical transition energies differ from the full valence CASSCF results by up to 0.2 eV. The absorption spectrum of B_4 will have strong bands (*cf*. transition moments in Table 5) to the $^1B_{2u}$ state starting around 2.20 eV and the $^1B_{3u}$ state around 3.82 eV. These states form a Jahn–Teller pair, the D_{4h} E_u structure is calculated to lie 2 eV and 1.45 eV above the equilibrium energies of the two rhombic components. Though the transitions to the Jahn–Teller pair in gerade symmetry are symmetry forbidden, they could gain intensity by

Table 7. Vertical (T_v) and adiabatic (T_e) excitation energies and transition moments (μ_e) between singlet states of C_{2v} B_4 and between doublet states of C_{2v} B_4^+.

	B_4					B_4^+			
	$T_{v,av}$ [a] [eV]	μ_e [debye]	T_v [b] [eV]	T_e [c] [eV]		$T_{v,av}$ [a] [eV]	μ_e [debye]	T_v [b] [eV]	T_e [c] [eV]
X $^1A_1$	0		0	0	X $^2A_1$	0			
A $^1A_1$	1.27	1.6832 (x)	1.35	0.41	A $^2B_2$	1.33	0.3485 (z)	1.37	1.15
B $^1B_1$	1.90	0.9179 (y)	1.76	1.50	B $^2A_1$	1.47	0.2443 (x)	1.52	1.32
C $^1B_2$	2.37	0.2348 (z)	2.21	2.01	C $^2B_1$	1.71	0.4057 (y)	1.76	1.06
D $^1B_2$	2.43	1.2223 (z)	N.C.		D $^2A_2$	1.94			
E $^1A_2$	2.50		2.53	2.35	E $^2B_2$	2.04	0.6730 (z)	2.03	1.93
F $^1B_1$	2.58	0.3910 (y)	2.61		F $^2B_1$	2.51	0.5600 (y)	2.58	2.51
G $^1A_2$	3.10		3.75		G $^2A_2$	2.73			

[a] Full-valence SA-CASSCF with aug-cc-pVTZ basis set at the optimized geometry of X $^1A_1$ (Table 3); two states per irreducible representation calculated.
[b] Full-valence CASSCF with aug-cc-pVTZ basis set at the optimized geometry of X $^1A_1$ (Table 3); each state calculated separately.
[c] Full-valence CASSCF with aug-cc-pVTZ basis set at optimized geometry (Table 3); each state calculated separately.

vibronic coupling via the b_{3u} mode with the close lying ungerade states (Table 5).

In B_4^+ two excited doublet states lie lower than the first quartet state (Table 6). As discussed, the $^2B_{1g}$ state is calculated only 0.17 eV above X ^2A_g and both are vibronically coupled. Due to possible intensity borrowing it is difficult to calculate reliable radiative transition probabilities for the absorption spectra. Nevertheless in the doublet states the most intense transitions should again be those to the Jahn–Teller states $^2B_{3u}$ and $^2B_{2u}$ for which the vertical energy difference is calculated to be about 3.1 eV. The computations of the stationary point in D_{2h} symmetry for the second $^2B_{2u}$ component (Table 2) did not converge because of the perturbation by other electronic states. Also the vertical energy differences for the quartet states are given in Table VI. The transition moments between these states are given relative to the lowest $^4B_{1g}$ state.

The C_{2v} minima are calculated higher than those of the rhombic isomers (Tables 1 and 2). In Table 7 the vertical and adiabatic excitation energies for these isomers are given. Providing that both rhombic and C_{2v} isomers coexist in the sample, the UV spectra will show transitions for both species. In B_4 the most intense transitions are calculated to the $^1A_1$, $^1B_1$ and $^1B_2$ states (Table 7), which lie much lower that the first allowed singlet transition in the rhombic isomer. This pattern should allow the isomers to be distinguished from their electronic spectra. In the case of B_4^+ the comparison of energy differences in Tables 6 and 7 shows that the pattern of electronic tran-

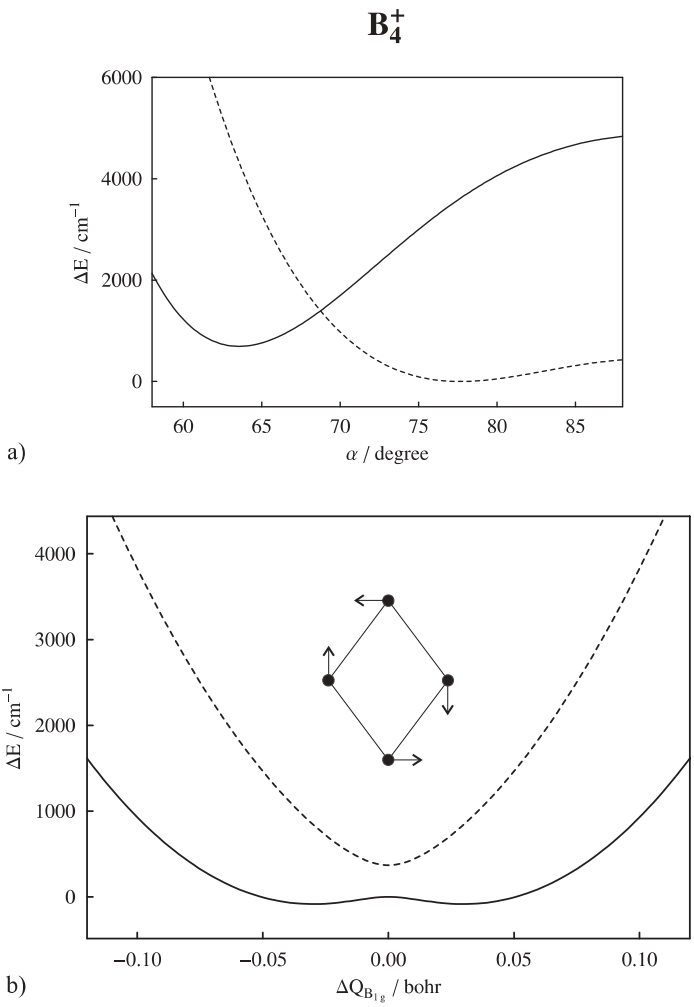

Fig. 2. One dimensional cut in D_{2h} symmetry along the ring angle coordinate and $R_e = 2.958$ bohr (cf. Table 2) of the ^2A_g and $^2B_{1g}$ states of B_4^+. Lower (broken line) and upper (full line) potentials correspond to the ^2A_g and $^2B_{1g}$ states respectively. In the SA-CASSCF calculations (cc-pVTZ, active space 3-5a_g, 2-3b_{3u}, 2-3b_{2u}, 1b_{1g}, 1-2b_{1u}, 1b_{2g}, 1b_{3g}) both states were averaged with equal weights. In lower part of the figure the avoided crossing along the B_{1g} coupling mode for $R_e^{\text{ref}} = 2.958$ bohr and apex angle of $\alpha^{\text{ref}} = 68$ degrees is shown.

sitions will make such an identification more difficult, though also in this case bands below about 1.5 eV will advocate the presence of the second isomer.

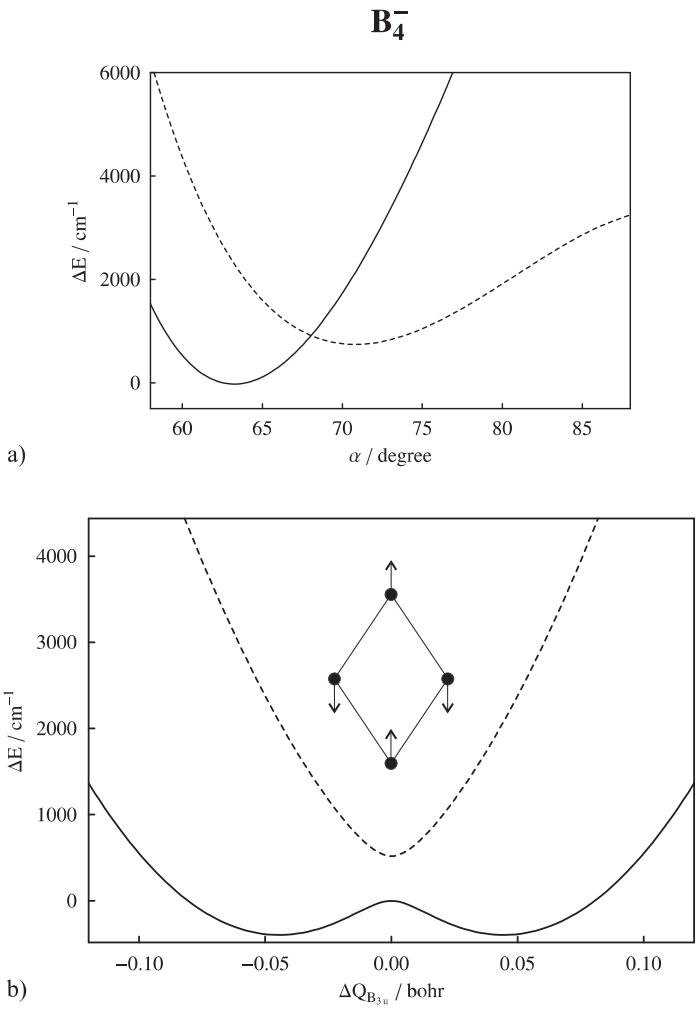

Fig. 3. One dimensional cut in D_{2h} symmetry along the ring angle coordinate and $R_e = 2.992$ bohr (cf. Table 2) of the ^2A_g and $^2B_{3u}$ states of B_4^-. Lower (full line) and upper (broken line) potentials correspond to the $^2B_{3u}$ and ^2A_g states respectively. In the SA-CASSCF calculations (cc-pVTZ, active space 3-6a_g, 2-3b_{3u}, 2-3b_{2u}, 1b_{1g}, 1b_{1u}, 1b_{2g}, 1b_{3g}) both states were averaged with equal weights. In lower part of the figure the avoided crossing along the B_{3u} coupling mode for $R_e^{\text{ref}} = 2.992$ bohr and apex angle of $\alpha^{\text{ref}} = 67$ degrees is shown.

4. Summary and conclusions

So far only the photodetachment spectrum of rhombic B_4^- [5] has provided experimental information on the singlet ground and excited triplet states of B_4 for

a comparison with theoretical results. The calculated full valence CASSCF excitation energies for the observed two lowest triplet states agree to within about 0.1 eV with the experimental band positions. A similar computational approach was employed to calculate vertical and adiabatic excitation energies up to about 4.5 eV for B_4 and B_4^+, including the electronic transition moments, which could aid the search for boron tetramers by electronic spectroscopy. In the rhombic ground state of the charged clusters the Born–Oppenheimer approximation fails; in B_4^+ the ^2A_g and $^2B_{1g}$ states are coupled by the b_{1g} vibration, in B_4^- the ^2A_g and $^2B_{3u}$ states by the b_{3u} mode.

Acknowledgement

This work has been supported by the Office of Aerospace Research and Development and the Swiss National Science Foundation (project 200020-100019). The continual advice and help on this project by Dr. W. C. Larson, AFRL Edwards California, has been much appreciated.

References

1. Y. M. Hamrick, R. J. Van Zee, and W. Weltner, J. Chem. Phys. **96** (1992) 1767.
2. S. Li, R. J. Van Zee, and W. Weltner, Chem. Phys. Lett. **262** (1996) 298.
3. M. Wyss, E. Riaplov, A. Batalov, J. P. Maier, T. Weber, W. Meyer, and P. Rosmus, J. Chem. Phys. **119** (2003) 9703.
4. P. Cias, M. Araki, A. Denisov, and J. P. Maier, J. Chem. Phys. **121** (2004) 6776.
5. J. Zhai, L.-S. Wang, A. N. Alexandrovna, A. I. Boldyrev, and V. G. Zakrzewski, J. Phys. Chem. A **107** (2003) 9319, and references therein.
6. L. Hanley, J. L. Whitten, and S. L. Anderson, J. Phys. Chem. **92** (1988) 5803.
7. S. A. Ruatta, L. Hanley, and S. L. Anderson, J. Chem. Phys. **91** (1989) 226.
8. P. A. Hintz, S. A. Ruatta, and S. L. Anderson, J. Chem. Phys. **92** (1990) 292.
9. J. Berkowitz and W. A. Chupka, J. Chem. Phys. **40** (1964) 2735.
10. S. J. La Placa, P. A. Roland, and J. J. Wynne, Chem. Phys. Lett. **190** (1992) 163.
11. M. B. Sowa-Resat, J. Smolanoff, A. Lapicki, and S. L. Anderson, J. Chem. Phys. **106** (1977) 9511.
12. H. W. Jin and Q. S. Li, Phys. Chem. Chem. Phys. **5** (2003) 1110, and references therein.
13. Q. S. Li and H. W. Jin, J. Chin. Chem. Soc. **50** (2003) 1115.
14. G. H. Jeong, R. Boucher, and K. J. Klabunde, J. Am. Chem. Soc. **112** (1990) 3332.
15. P. A. Hintz, M. B. Sowa, S. A. Ruatta, and S. L. Anderson, J. Chem. Phys. **94** (1991) 6446.
16. A. C. Tang, Q. S. Li, C. W. Liu, and J. Li, Chem. Phys. Lett. **201** (1993) 465.
17. A. Ricca and C. W. Bauschlicher Jr., Chem. Phys. **208** (1996) 233.
18. Z. X. Wang and M. B. Huang, J. Am. Chem. Soc. **120** (1988) 6758.
19. J. E. Fowler and J. M. Ugalde, J. Phys. Chem. A **104** (2000) 397.
20. E. D. Jemmis and M. M. Balakrishnarajan, J. Am. Chem. Soc. **123** (2001) 4324.
21. A. N. Alexandrova, A. I. Boldyrev, H.-J. Zhai, L.-S. Wang, E. Heiner, and P. W. Fowler, J. Phys. Chem A **107** (2003) 1359, and references therein.
22. Q. S. Li, L. F. Gong, and Z. M. Gao, Chem. Phys. Lett. **390** (2004) 220.
23. I. Boustani, Phys. Rev. B **55** (1997) 16426.

24. I. Boustani, Chem. Phys. Lett. **233** (1995) 273.
25. H. Reis and M. G. Papadopoulos, J. Comput. Chem. **20** (1999) 679.
26. J. M. L. Martin, J. P. Francois, and R. Gijbels, Chem. Phys. Lett. **189** (1992) 529.
27. H. Kato and E. Tanaka, J. Comput. Chem. **12** (1991) 1097.
28. H. Kato and E. Tanaka, J. Chem. Soc. Japan (Nippon Kagaku Zasshi) **8** (1989) 1183.
29. A. K. Ray, I. A. Howard, and K. M. Kanal, Phys. Rev. B **45** (1992) 14247.
30. R. Linguerri, I. Navizet, P. Rosmus, S. Carter, and J. P. Maier, J. Chem. Phys. **122** (2005) 34301.
31. C. L. Yang, Z. H. Zhang, T. Q. Ren, R. Wang, and Z. H. Zhu, J. Mol. Struct. (Theochem) **583** (2002) 63.
32. MOLPRO is a package of *ab initio* programs written by H.-J. Werner and P. J. Knowles: further information from http://www.molpro.net/.
33. H.-J. Werner and P. J. Knowles, J. Chem. Phys. **82** (1985) 5053; Chem. Phys. **115** (1985) 259.
34. J. F. Stanton and R. J. Bartlett, J. Chem. Phys. **98** (1993) 7029.
35. P. J. Knowles, C. Hampel, and H.-J. Werner, J. Chem. Phys. **99** (1993) 5219; Erratum: J. Chem. Phys. **112** (2000) 3106.
36. T. H. Dunning, J. Chem. Phys. **90** (1989) 1007; R.A. Kendall, T. H. Dunning, and R. J. Harrison, J. Chem. Phys. **96** (1992) 6796.